ANALYSIS OF FRACTURE GROWTH MODELS FOR HYDRAULIC FRACTURING OF SHALE GAS DEPOSITS IN THE KAROO, SOUTH AFRICA

Prepared by

Patrick Atwine Tumureebire

670161

A research report submitted in partial fulfilment of the requirements for the degree of

Master of Science in Chemical Engineering, Oil and Gas option, by coursework and research report

Submitted to

School of Chemical and Metallurgical Engineering, Faculty of Engineering and the Built Environment, University of the Witwatersrand, Johannesburg, South Africa

Supervisor: Dr D. Nkazi

21 October 2019

Plagiarism Declaration

I______**PATRICK ATWINE TUMUREEBIRE**_____________________

(Student number: __**670161**_____________________) am a student registered for ___**CHMT 7008A**_____________

in the year __**2018**________. I hereby declare the following:

- I am aware that plagiarism (the use of someone else's work without their permission and/or without acknowledging the original source) is wrong.
- I confirm that the work submitted for assessment for the above course is my own unaided work except where I have explicitly indicated otherwise.
- I have followed the required conventions in referencing the thoughts and ideas of others.
- I understand that the University of the Witwatersrand may take disciplinary action against me if there is a belief that this is not my own unaided work or that I have failed to acknowledge the source of the ideas or words in my writing.

Student Signature: Date: ______________

Abstract

Prediction of fracture dimensions during propagation of a hydraulically induced fracture for well stimulation is essential for the design of a stimulation treatment. This study seeks to better understand the mechanisms of hydraulic fracturing through computational modelling of the fracture growth up to a specific time in MATLAB.

The computations were based on three existing theories of fracture propagation: the Khristianovitch, Geertsma and de Klerk (KGD) model, Perkins and Kern model (PKN) and Pseudo 3D model. Owing to the absence of raw data for the Whitehill formation in the Karoo, analogous shale rock from the United States of America was used as a basis for the study. The MATLAB computations were thus performed based on the following rock properties: Shear modulus = 1.466 x 10^5Psi; Drained Poisson's ratio = 0.2; Fluid Viscosity = 1cp; Pumping rate = 62.5bbl/min; In-situ stress = 3200Psi; Wellbore radius = 0.2ft; Passed time = 0.3min.

This report documents the differences in height, length, width, and pressure, predicted by the 2D and 3D models for the same set of input parameters. It is shown that the growth of the fracture for the 2D models yield much shorter lengths than the 3D model. It is also seen that the wellbore pressure predicted by the PKN model, in contrast to the KGD model, increases to 2.564 x 10^5 psi. as the fracture length increases. The pressure predicted by the P3D model increases to a peak of 1.411 x 10^6 psi at t = 0.24sec before declining to a final 7.709 x 10^5 psi.

Though the report proposed an understanding of the mechanisms of hydraulic fracturing in the Karoo, and even obtained solutions, it is limited to simulation models without application to field data.

Acknowledgements

I truly believe that this report is a culmination of the immense support I have received from several people. To name a few, I would like to acknowledge and thank my parents and siblings for their continued care and aid throughout the duration of this work. My supervisor for his consistent feedback and guidance through each phase of this project. CHIETA and the NRF for their financial assistance when it mattered most. And lastly, my community of friends who have now become family for their ever-present help when I have needed them most. I am truly grateful.

Contents

List of Figures

List of Tables

Nomenclature

A	=	cross-sectional area
E	=	Young's modulus
G	=	shear modulus
g	=	gravitational acceleration constant
K	=	permeability
P_{BD}	=	breakdown pressure
P_{pore}	=	pore pressure
q	=	gas flowrate
ρ	=	density
μ	=	viscosity
ρ_f	=	fluid density
σ_v	=	vertical stress
σ_h	=	minimum horizontal stress
σ_H	=	maximum horizontal stress
σ_t	=	tectonic stress
$\sigma_1, \sigma_2, \sigma_3$	=	principal stresses
$\sigma_x, \sigma_y, \sigma_z$	=	normal stresses in global coordinate system
σ_{avg}	=	average in-situ stresses

Chapter 1: Introduction

1.1 Background

Hydraulic fracturing is the breaking of rocks by injection of a fluid at a high pressure (Wangen, 2017). It is an important method used in the exploration of oil and gas (McClure, 2012). This is because the ability of a well to produce hydrocarbons or receive injection fluids is limited by the reservoir's natural permeability. Hydraulic fracturing therefore seeks to improve hydrocarbon flow by creating pathways in the formation that connect the reservoir and wellbore (Nolen-Hoeksema, 2013). Its application in the oil and gas industry over the last 5 decades has been to enhance the connection between a well and a productive reservoir. In other environments, it is used to create or stimulate already existing fractures in a low permeability matrix (Howard & Fast, 1970). An example of the latter is the stimulation of shale-gas reservoirs in order to extract gas (Geel, Schulz, Booth, de Wit, & Horsfield, 2013) as seen in Figure 1.1. Further engineering applications of hydraulic fracturing include: energy extraction from geothermal reservoirs, rock mass pre-conditioning and/or de-stressing in mining, and measurement of underground in situ stress state (Dandekar, 2013).

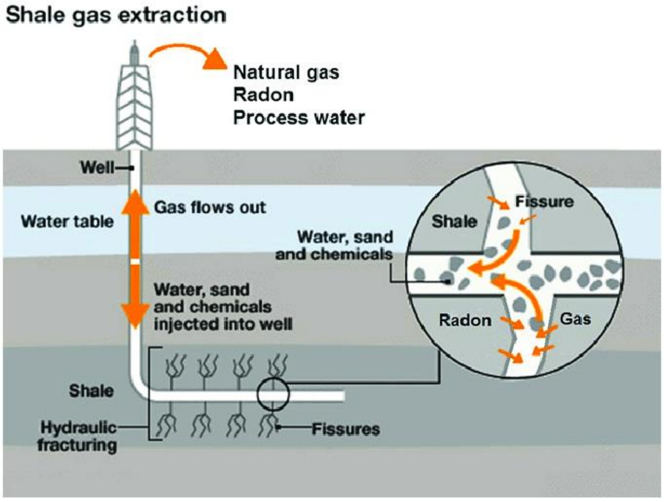

Figure 1.1: Diagram depicting the process of hydraulic fracturing used to extract shale gas (Li, Xing, Liu, & Liu, 2015)

Complicated geological settings, such as, local heterogeneities or a complex in situ stress field, contribute to the challenging task of hydraulic fracturing (Figueiredo, Tsang, Rutqvist, & Niemi, 2017). The low permeability natures of these unconventional reservoirs also add to the complexity of the challenge. In order to optimise gas recovery from such reservoirs, it is important to investigate and understand how hydraulic fracturing is done in these settings.

Numerical modelling thus also plays an important role because such conditions cannot be reproduced by laboratory experiments.

A resource assessment conducted by Decker & Marot (2012), shows that the Southern Karoo has potential reserves of between 32 to 485 trillion cubic feet (tcf). This puts South Africa even further on the map as having the fifth largest technically recoverable shale gas resource in the world. Table D.1 in appendix D depicts this clearly. The ability to harness this resource will bring South Africa one-step closer to solving several energy issues. In addition to this, it will also provide sustainable alternatives to the already exhausted and environmentally pollutive non-renewable dependants.

This research will use work done by Nasiri (2015), which covers fracture growth modelling in MATLAB, and Yildrium, (2014) which investigates petrophysical properties of Marcellus shale, as a reference point. This will help in the initial understanding of how to accurately model the fracture growth process. In instances where petrophysical and geological data from a sample of shale rock in the Karoo is unavailable, analogous, Marcellus shale rock will provide the necessary data to populate the model.

1.2 Problem Statement

The challenge is to understand the process model of hydraulic fracturing on the conditions of the Karoo under its complex geological setting.

To be able to solve this problem, an understanding of the model process is essential for the design fracture operations. Because of the current socio-economic issues regarding fracking in the Karoo as well as the confusion around the Mineral and Petroleum Resources Act (MPRDA) Amendment Bill, obtaining exact raw data from the Karoo is not possible. In the absence of raw data, analogues from a geological setting exhibiting similar characteristics as that of the Karoo can be used to populate the model.

The mineralogy, shale formation and other petrophysical and geological data from the Karoo form the foundation upon which fracture propagation and reservoir models are constructed. Examining this will provide better means of understanding the extent to which gas can be extracted the process optimised.

Understanding this will then aid in the advancement of fracking in South Africa. The region within the Karoo that will be considered is outlined in Chapter 2.

1.3 Research Objectives

In the design of a hydraulic fracturing operation, there are two mechanisms that need to be considered: initiation and propagation of the hydraulic fracture. Careful consideration of factors that influence these two mechanisms in the context of an unconventional reservoir, in a complex geological setting, will provide a means to improve understanding of and effectively design the fracture process. For the purposes of this research, models concerning only the initiation of the fracture, in the context of the Karoo, will be studied.

The following objectives highlight the focus of this project:

- Enhance understanding of the mechanisms of hydraulic fracturing, specifically in the Karoo, through means of computational modelling.
- To represent the growth of a fracture for hydraulic fracturing of shale rock in the Karoo.
- Analyse and solve the equations of models that best represent fracture growth to its final shape at a specific time.

Chapter 2: Literature Review

2.1 Shale gas and Fracking in SA

Currently, hydraulic fracturing is not done in South Africa. There has been hesitation to adopt the process due to the drawbacks of immense water consumption and the potential of groundwater contamination. Civil society groups and communities, rallying behind slogans such as “Don’t Frack with Our Karoo!” (Nell, 2017), have contributed to the outcry against the process. In addition; baseline studies, logistical, political and socio-economic structures still need to be refined for exploration in the Karoo to commence (O'Connor, et al., 2016).

Despite the insufficient research as well as the lack of a regulatory oversight and legalistic framework for potential fracking, applications for work aimed at determining the presence of a petroleum resource are well under way. A comprehensive and analytical study conducted by the Development Bank of South Africa (DBSA) (2014) revealed that the existing shale gas reserve could be a ‘transformational opportunity’ for South Africa and for those that rely on it for their livelihood. This demands a proper assessment of the reserve because confirmed shale gas deposits could contribute significantly to economic development across a spectrum of industries. “The cost of extracting shale gas from the Karoo would be outweighed by the benefits to the South African economy in terms of potential jobs and industrial development.” (DBSA, 2014) The question, then, is not a matter of whether the practice should be carried out, but rather, how it should be done. Understanding this complex process within the bounds of the Karoo climate will provide a way forward to ensuring its success.

Despite reservations in some countries, the practice of fracking has been successfully tested and tried throughout the world. North America has been the most successful. It is currently the leading innovator in terms of fracking (O'Connor, et al., 2016). There is compelling evidence as presented by Fakir (2015), to show that though this process is successful, it is not exactly replicable everywhere in the world, owing to the complexity and uniqueness of each geological setting, and the type of formations found along with the varying rock characteristics. On top of this, few numerical studies have been performed in comparison to the number of experiments carried out to further analyse the mechanisms of hydraulic fracturing on the particular conditions under consideration (Li, Xing, Liu, & Liu, 2015). It is therefore imperative to have a wider view of the rock matrix and other petrophysical data that describe the shale formation in the Karoo; as well as an understanding of the process itself – or at least part of it.

With particular attention to fracking of shale rock, one of the challenges that influence stimulation and productivity is the heterogeneous characteristics of the shale formations. It is because of this that shale gas characteristics of Permian black shales in the Ecca Group, near Jansenville in the Eastern Cape (South Africa) were studied in order to verify the potential for shale gas in the area (Geel, Schulz, Booth, de Wit, & Horsfield, 2013). The study reported on the geochemical and petrophysical properties of the black shales from the Prince Albert, Whitehill and Collingham formations of the Lower Karoo Supergroup, near Jansenville. Petrographic, XRF, XRD, and SEM analyses from the black shale of the Whitehill Formation revealed several underlying factors and characteristics, which confirm deltaic depositional model for the lower Ecca Group (Geel, Schulz, Booth, De Wit, & Horsfield, 2013).

Petrophysical analyses that were performed indicate that properties such as brittleness and porosity of the Whitehill Formation, although not as good as the under- and over-lying formations, would facilitate hydraulic fracturing and extraction of gas from these rocks. The Whitehill formation (Permian Shale, South Eastern Karoo Basin, Greystone area, RSA) was also compared with Barnett formation (Mississippian shale, Fort Worth Basin, USA) and Marcellus formation (Devonian Shale, Appalachian Basin USA) which revealed that characteristic properties of the Whitehill Formation as a shale gas host compared favourably with those of the currently exploited gas fields in the United States. This result will form part of the foundation for being able to construct a model in the context of raw data uncertainty.

2.2 Significance Pertaining to Fracture Growth

The two prominent issues that exist with fracking relate to initiation and propagation: breaking the rock, and the way in which fractures extend. Both occur deep within the earth and cannot be observed directly. Among many factors that affect hydraulic fracturing response, the properties of reservoir rock, fracture fluid and the magnitude and direction of in-situ stress play a significant role in allowing for an accurate prediction of the dimension (opening width, length, and height) of the hydraulically induced fracture for a given pumping rate and time (Weijers, De Pater, Owens, & Kogsboil, 1994).

As stated in 'Fracture Growth in Layered and Discontinued Media' by Warpinski (2011), the geometry of a hydraulic fracture depends strongly on both the mechanical properties of the rock formation, which describe how the formation will deform under a change in stresses, and the stresses acting on the formation.

2.2.1 In-Situ Stress

Of the multiplicity of factors that influence hydraulic fracture growth, in-situ stress has the most significant effect on fracture height growth. The importance of stress was noted early on (Perkins & Kern, 1961) and has been widely considered in modelling (Linkov, 2014), and numerous laboratory experiments. Fracture height growth can be easily restricted if the layers above and have higher stress than the reservoir rock, and this is a common occurrence in sedimentary basins. An equilibrium (static) analysis of the Linear Elastic Fracture Mechanics behaviour of a fracture surrounded by rocks with higher stress was first given by Simonson et al. (1978) for a symmetric case, which stated that stresses above and are equal. Given the geometry in Figure 2.1, an equation can be written as:

$$\sigma_2 - P = \frac{2}{\pi}[\sigma_2 - \sigma_1] \sin^{-1}\left(\frac{h}{H}\right) - \frac{K_{Ic}}{\sqrt{\pi H/2}}$$

Equation 2. 1: Stress effects equation based on Figure 2.1.

Where:

P = net pressure in fracture

σ_1 = pay zone stress

σ_2 = stress in boundary layers

h = pay zone thickness

H = total fracture height

K_{Ic} = fracture toughness of the boundary layers

In this equation, the first term on the right is due to the stress contrasts, while the second term is due to fracture toughness. For standard laboratory values of fracture toughness, the term on the left is generally small and the height of the fracture is mostly dependent on the stress contrasts. In general, this equation is conservative since there are other dynamic factors that affect the amount of height growth that will occur. Similar equations can be developed for non-symmetric stress contrasts, but more complete dynamic analyses are usually performed in fracture models (Warpinski N. , 2011).

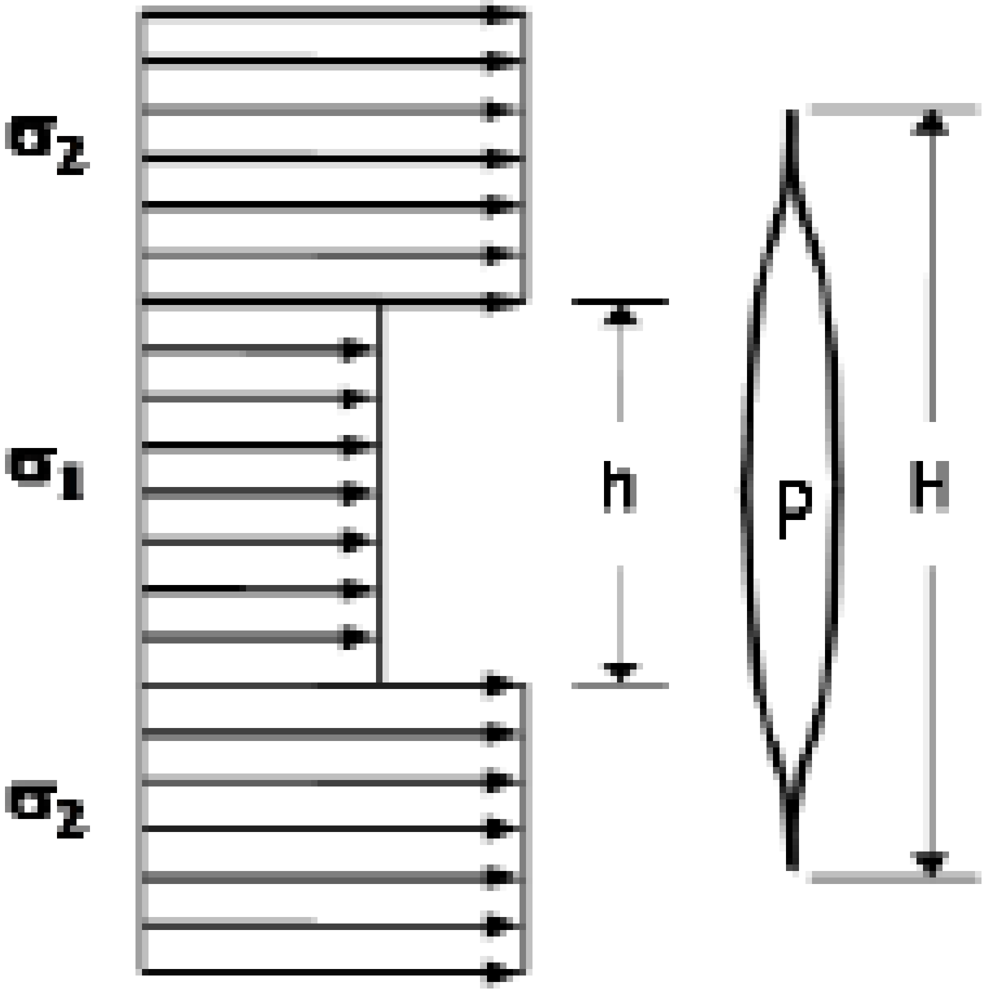

Figure 2. 1: Geometry for stress effects.

2.3 Pressure and Stresses

The size and orientation of a fracture, and the magnitude of the pressure needed to create it, are dictated by the formation's in-situ stress field. This stress field may be defined by three principal compressive stresses, which are oriented perpendicular to each other (Illustrated in Figure 2.2). The magnitudes and orientations of these three principal stresses are determined by the tectonic regime in the region and by depth, pore pressure and rock properties, which determine how stress is transmitted and distributed among formations (Dandekar, 2013). The geometry of a hydraulic fracture depends strongly on both the mechanical properties of the rock formation, which describe how the formation will deform under a change in stresses, and the stresses acting on the formation (Desroches & Bratton, 2000). These three stresses as defined by Wangen (2017), in 'A 2D Volume Conservative Numerical Model of Hydraulic Fracturing', are:

1) Vertical stress – given by the weight of overburden, is expressed as:

$$\sigma_v = \int_0^D \rho(z) g dz$$

$$\sigma_v = \rho g D$$

Equation 2. 2: Vertical stress given by overburden weight

Where: ρ = density of the material

D = depth in z-axis pointing vertically downward

Note: average overburden density = 15-19.2ppg

2) Pore pressure – derived from the pore fluid trapped in the void spaces in the rocks; can be normal or abnormal; carries part of the total stresses applied to the system while matrix carries the rest.

$$P_{f,n} = \rho_f g D$$

Equation 2. 3: Pore pressure derived from the pore fluid trapped in rock void spaces

Where: ρ_f = fluid density

For brine, average pore fluid density = 8.76ppg

Normal pressure ranges from 0.447-0.465psi/ft; it averages 0.0105MPa/m

3) Horizontal stress – where no rigidity is concerned (i.e. the ocean), vertical and horizontal stresses are the same. In a formation, they differ (because of rigidity)

$$\sigma_H = \sigma_h + \sigma_{tect}$$

Equation 2. 4: Horizontal stress (excl. rigidity)

Superscripts: H = maximum horizontal stress

h = minimum horizontal stress

tect = tectonic stress

$$\sigma_v > \sigma_H > \sigma_h$$

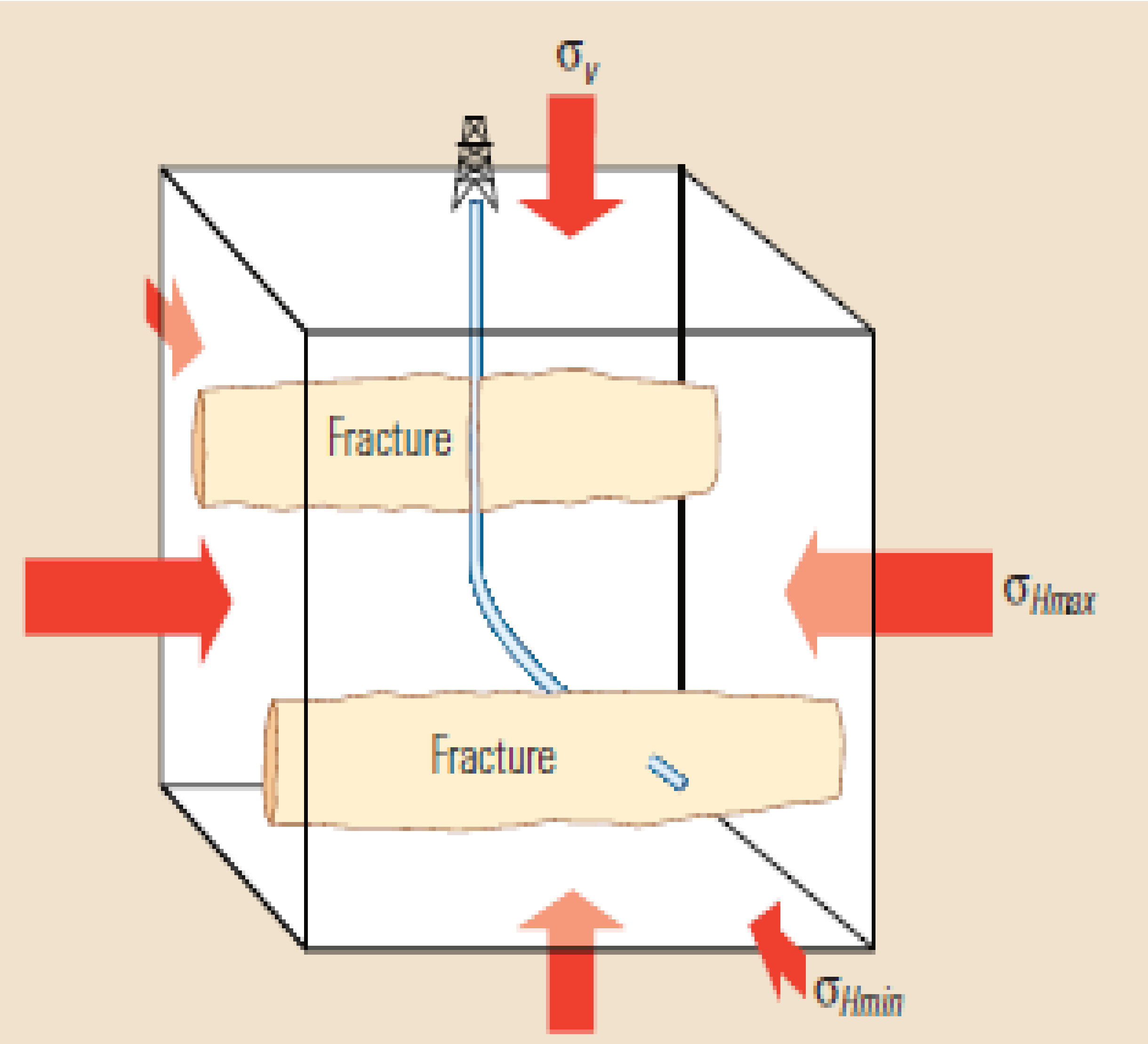

Figure 2. 2: 3D representation of the three principal compressive stresses involved in the initiation and propagation of hydraulic fracturing (Nolen-Hoeksema, 2013)

In-situ stresses control the orientation and propagation direction of hydraulic fractures. Hydraulic fractures are tensile fractures, and they open in the direction of least resistance. If the maximum principal compressive stress is the overburden stress, then the fractures are vertical, propagating parallel to the maximum horizontal stress when the fracturing pressure exceeds the minimum horizontal stress. The three principal stresses increase with depth. The rate of increase with depth defines the vertical gradient. The principal vertical stress, commonly called the overburden stress, is caused by the weight of rock overlying a measurement point. Its vertical gradient is known as the lithostatic gradient. The minimum and maximum horizontal stresses are the other two principal stresses. Their vertical gradients, which vary widely by basin and lithology, are controlled by local and regional stresses, mainly through tectonics (Adachi, Detournay, & Peirce, 2010).

The weight of the fluid above a measurement point in normally pressured basins creates in situ pore pressure. The vertical gradient of pore pressure is the hydrostatic gradient. However, pore pressures within a basin may be less than or greater than normal pressures and are designated as under-pressured or over-pressured, respectively (Wangen, 2017).

Figure 2.3 shows what happens to the pressure beyond fracture initiation. During a stimulation treatment, engineers pump fluid into the targeted stimulation zone at a prescribed rate (blue polygons), and pressure (red line) builds to a peak at the breakdown pressure, then it drops, indicating the rock around the well has failed. Pumping stops, and pressure decreases to below the closure pressure. During a second pumping cycle, the fracture opens again at its reopening pressure, which is higher than the closure pressure. After pumping, the fracture closes and the pressure subsides. The initial pore pressure is the ambient pressure in the reservoir zone (Nolen-Hoeksema, 2013).

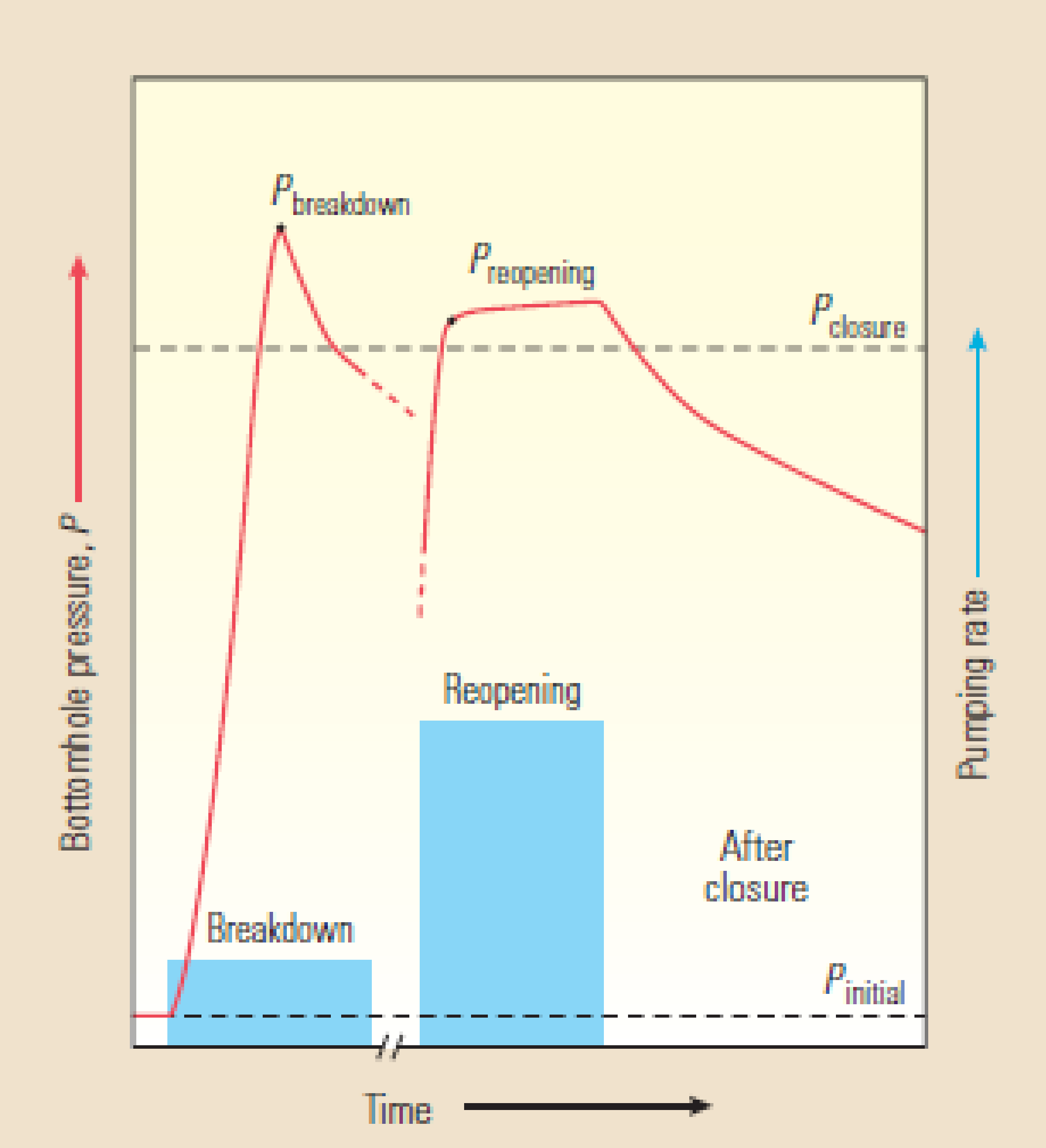

Figure 2. 3: Graphical depiction of pressures during a fracture treatment (Nolen-Hoeksema, 2013).

A more detailed pressure profile of the pressure measured inside the hole near the opening of a hydraulic fracture is shown and explained in Appendix A

2.4 Fluids Used in Fracking

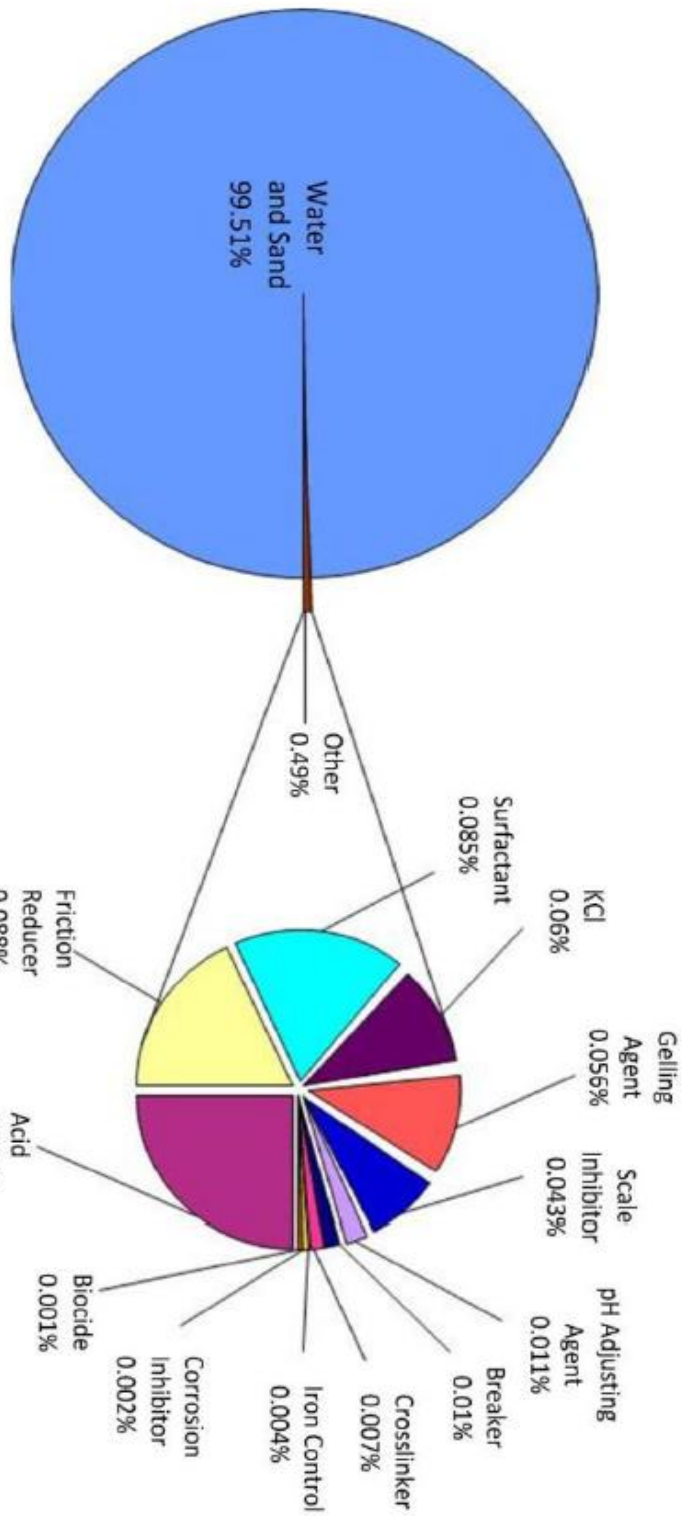

Figure 2. 4: Volumetric composition of a typical fracturing fluid, Fayetteville, Arkansas, USA (Brookes, Cohen, Morris, & Orme-Zavaleta, 2014)

Chemical additives in the fracture stimulation fluid are highly diluted so they only represent less than 1% of the volume of the fluid, as shown in Figure 2.4.

Categories of fracturing fluids available usually consist of:

- Viscosified water-based fluids
- Non-viscosified water-based fluids
- Gelled oil-based fluids
- Acid-based fluids
- Foam fluids

Table D.2 in appendix D lists the types of fracturing fluids that are available and the general use of each type of fluid. Reasons for selecting between these fluid types will depend on a variety of factors, such as its main composition, particular use, base fluid, etc, as outlined in Table D.2. For most reservoirs, water-based fluids with suitable additives are most appropriate, due to the historic ease with which large volumes of mix-water can be acquired. In some cases, foam generated with N_2 or CO_2 can be used to stimulate shallow, low-pressure zones successfully (Frink, 2013). When water is used as the base fluid, the water should be tested for quality due to some sensitivity of certain fluid chemistries to the mix-water composition (Howard & Fast, 1970).

2.5 Numerical Modelling

Though modelling is used to develop an improved understanding of the fracking process, an adequate, fundamental understanding of the process to be modelled is required. As previously mentioned, the entire process of hydraulic fracturing is rather complex, even in its most basic form, but can be broken down into three main physical processes:

1) Mechanical deformation of fracture surfaces

2) Fluid flow within the fracture

3) Fracture propagation

As Noted by Adachi et al., (2007), each of the above physical processes can be described by their relative scientific laws respectively:

1) Linear elasticity: this is represented by an integral equation that determines the non-local relationship by measuring the fracture width and fluid pressure.

2) Lubrication theory: represented by a non-linear partial differentiation equation that relates the fluid flow velocity, fracture width and pressure gradient. The leak-off effects are accounted for by the additional term added to the equation.

3) Linear elasticity fracture mechanics theory (LEFM): this describes the fact that the fracture will propagate if the stress intensity factor at the tip matches the rock roughness.

A numerical method will be used as a tool to better represent the essential mechanism of hydraulic fracturing in an appropriate manner so as to aid understanding and design while remaining computationally feasible (Li, Xing, Liu, & Liu, 2015). There are several theoretical models that have been developed over the last 50 years. The progression thereof and a brief description of each is outlined as follows:

Classic 2D models – PKN model (assumes plain strain in vertical direction; when fracture length is much greater than the height) and KGD model (assumes crack width in horizontal direction is independent of the vertical position) as per Howard & Fast (1970).

Pseudo 3D (P3D) models were developed to investigate the fracture propagation vs height based on the PKN model. The two categories of P3D models are cell-based and lumped model. The main issue, as outlined by Howard & Fast (1970), is that neither of these are useful for simulating fracturing process with arbitrary shapes.

Hence Planar 3D (PL3D) models were developed. An assumption of this model is that the shape of the fracture is arbitrary and can be represented by Green's function (Hattori, Trevelyan, Augarde, Coombs, & Aplin, 2017). This model is slightly more representative and considers real conditions but is still not sufficient, because it requires a consistency condition between layers (Wang, Li, & Zhang, 2016; Wangen, 2017). This means that 'out of plane' fractures cannot be modelled, and the use of Green's function makes it difficult for nonlinear or anisotropic rocks to be simulated.

Thus, Finite Element Modelling (FEM) was developed to simulate real-time fractures and avoid singularity issues. However, the major shortfall with this model is that it is unable to predict fracture orientation under complex stress conditions such as re-orientation. The solution to this inadequacy was solved by Adachi et al. (2007), Li, Xing, Liu, & Liu (2015) where the results of their findings showed that it is best to implement FEM with continuum damage mechanics.

Other methods that have been used to numerically simulate the hydraulic fracturing process of hydraulic fractures include the extended Finite Element Method (XFEM) and Discrete Fracture

Network (DFN) (Li, Xing, Liu, & Liu, 2015; Wang, Li, & Zhang, 2016). The XFEM has been implemented on the effects of intersection angles between hydraulic fractures and natural fractures (Taleghani & Olson, 2009). However, some downfalls to this method include the branching of intersection of fractures, fluid flow related to fractures and the heterogeneities of rocks. By DFN, one is able to consider fluid flow and fracture mechanics within the fracture; although there are also some limitations on the angle between the fractures (Li, Xing, Liu, & Liu, 2015).

Lastly, looking at Displacement Discontinuity Method (DDM) and Boundary Element Method (BEM), it is harder to solve problems using these methods when there are several layers of rocks. Reason for this is explained due to the fact that applying continuity conditions on the bond between rocks, the solution becomes complex and will severely restrict the problem size (McClure, 2012).

As outlined in the work done by Nasiri (2015), Matlab will be used to simulate 2D and P3D hydraulic fractures with equilibrium height growth across stress barriers. The most common and simplest approach has been to use the local net fluid pressure, in-situ stress contrast, and rock toughness by satisfying the local static equilibrium to determine the fracture height. A constant fluid pressure is usually assumed over the vertical cross section of the fracture and the fluid flow is one dimensional along the direction of pay zone.

It is imperative to note that even though these models have been useful tools, under certain circumstances such as a formation (which has a complex in-situ stress distribution) the P3D fracture model may not be capable of capturing all important features due to the approximative nature of the model (Adachi, Detournay, & Peirce, 2010).

2.6 PKN, KGD and P3D Models

Widespread work has been done to simulate the fracture propagation and dimensions. There are multiple analytical and numerical models available in literature for estimating fracture dimensions, propagation and recession with different geometries as outlined in the previous section. The focus, however, will be mainly on the 2D models (PKN and KGD) and the P3D model.

2.6.1 PKN model

Perkins and Kern (1961) developed equations to compute fracture length and width with a fixed height. Later Nordgren (1972) enhanced this model by adding fluid loss to the solution; hence, this model is commonly called the PKN model. An assumption of this model is that fracture toughness could be neglected. This is because the energy required for the fracture to propagate was significantly less than that required for fluid to flow along the fracture length. What also adds to this assumption is with regards to the plane strain behaviour in the vertical direction as well as the constant height of the fracture and propagation along the horizontal direction, as seen in Figure 2.5.

From the aspect of solid mechanics, when the fracture height "h_f" is fixed and is much smaller than its length, the problem is reduced to two-dimensions by using the plane strain assumption (Xiang, 2011). For the PKN model, plane strain is considered in the vertical direction, and the rock response in each vertical section along the x-direction is assumed independent on its neighbouring vertical planes. Plain strain implies that the elastic deformations (strains) to open or close or shear the fracture, are fully concentrated in the vertical plane's section perpendicular to the direction of fracture propagation. This is true if the fracture length is much larger than the height.

From the aspect of fluid mechanics, fluid flow problem in PKN model is considered in one dimension in an elliptical channel. The fluid pressure, P_f , is assumed to be constant in each vertical cross section perpendicular to the direction of propagation (Xiang, 2011).

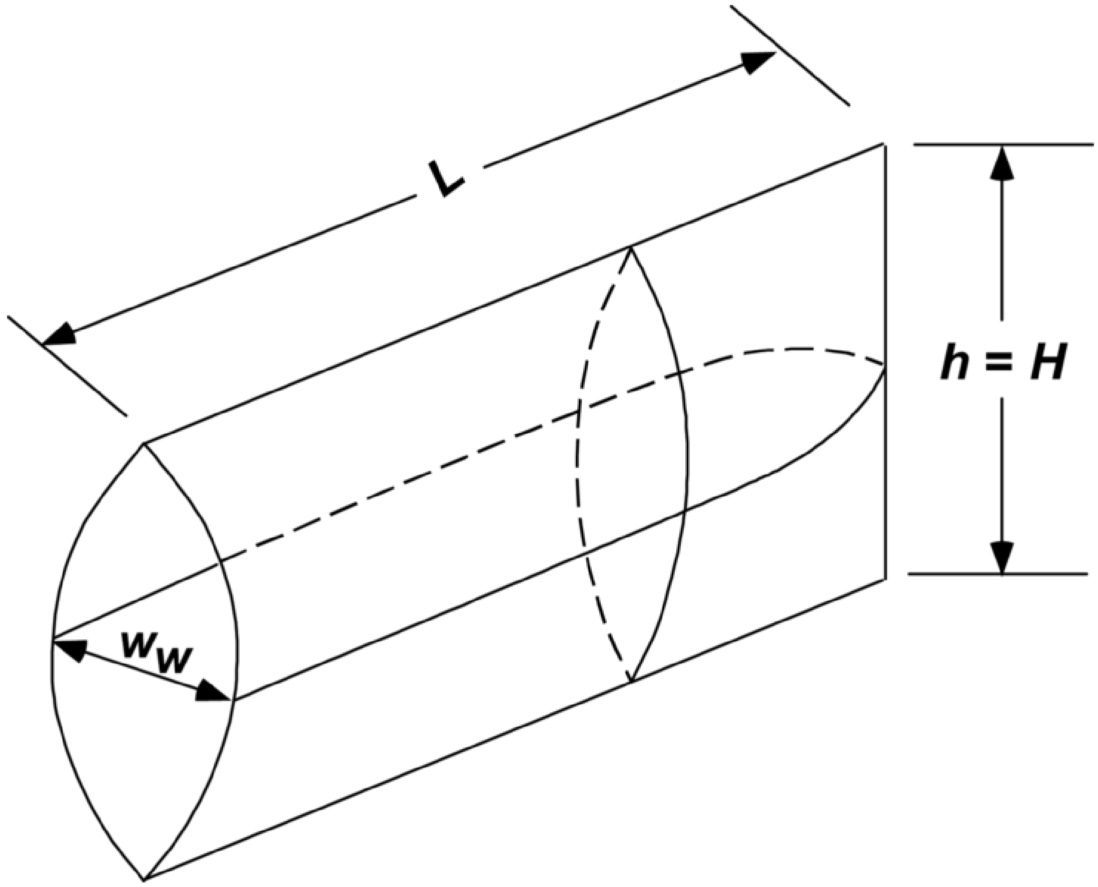

Figure 2. 5: PKN geometry for a 2D fracture, for when fracture length is greater than fracture height (Gidley, Holditch, Nierde, & Veatch, 1989)

2.6.2 KGD model

The KGD model was developed by Khristianovitch and Zheltov (1955) and Geertsma and de Klerk (1969). It considers fracture mechanics' effects on the fracture tip and simplifies the solution by assuming that the flow rate in the fracture is constant, and the pressure along the majority of the fracture length is also constant – except for a small region close to the tips (Li, Xing, Liu, & Liu, 2015). In this model, plane strain is assumed to be in horizontal direction; i.e., all horizontal cross sections act independently. This holds true only if fracture height is much greater than fracture length. In addition, since it assumes that the fracture width does not change along the fracture face, all sections are identical. The model also assumes that fluid flow and fracture propagation are in one dimension as seen in Figure 2.8.

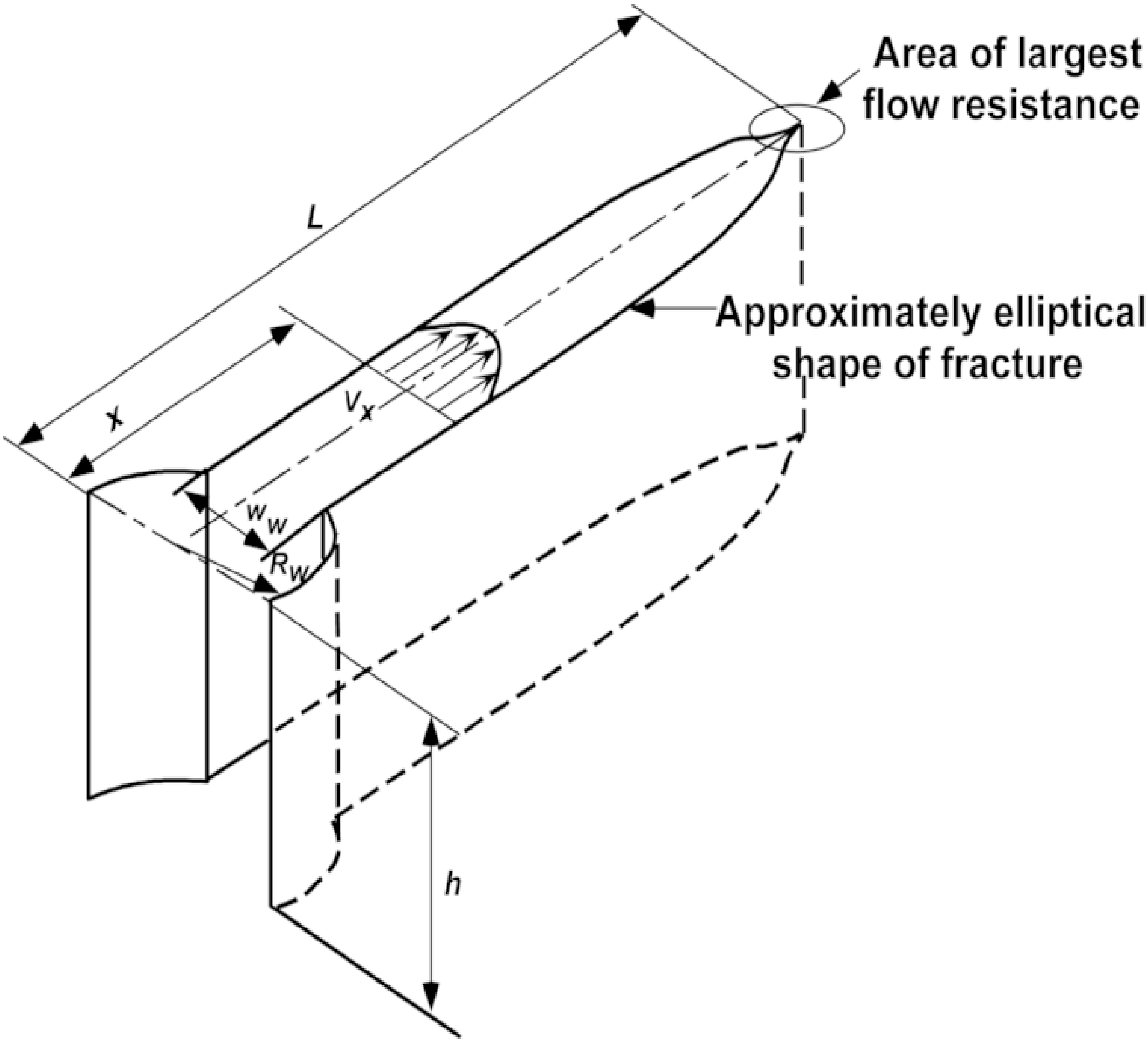

Figure 2. 6: KGD geometry for a 2D fracture, for when fracture height is greater than fracture length (Gidley, Holditch, Nierde, & Veatch, 1989)

The KGD model has six assumptions according to Gerrtsma & De Klerk (1969):

1) The fracture has an elliptical cross section in the horizontal plane.

2) Each horizontal plane deforms independently.

3) Fracture height, h_f, is constant.

4) Fluid pressure in the propagation direction is determined by flow resistance in a narrow, rectangular, vertical slit of variable width.

5) Fluid does not flow through the entire fracture length.

6) Cross sections in the vertical plane are rectangular (fracture width is constant along its height).

Since the fracture is assumed to be at a plane strain condition in the horizontal plane, the KGD model is best suited for fractures whose length/height ratio is near unity or less (Yew & Weng, 2015).

2.6.3 P3D model

The 2D fracture models discussed in the previous sections have been reasonably successful in practical simulation with a simplified calculation. However, they have limitations in that they are required to specify fracture height and/or assume radial fracture geometry to perform them. To solve that problem, pseudo-3D models are formulated by removing the assumption of constant and uniform height (Morales & Abou-Sayed, 1989). Instead, the height in pseudo-3D models is a function of position along the fracture and simulation time. Different from 2D models, a vertical fluid-flow component is added in pseudo-3D models. Fracture lengths must be much greater than fracture heights. The fully 3D models are even more complex and are introduced to handle fractures of arbitrary shape and orientation by removing the assumptions in pseudo-3D models (Rahman & Rahman, 2010).

Table D.3 in appendix D is a brief outline of each of the 2D and 3D models showing their equations, assumptions and approximate geometries. Derivations of the KGD and PKN can be found in Appendix C1 and C2.

The PKN model is a more appropriate approximation for fractures where the length is considerably longer than the height, and the KGD model should be used for fractures where the fracture length is of the same order or shorter than the fracture height (Smith & Shlyapobersky, 2014).

2.7 Modelling fracture growth

In order to model fracture growth, accurate knowledge of the in-situ stresses that exist within the formation need to be known. This will allow for the rupture or breakdown pressure – "the pressure at which the rock matrix of an exposed formation fractures and allows fluid to be injected" (Smith & Shlyapobersky, 2014) – to be obtained. In order to determine the breakdown pressure required to initiate the fracture, properties of the rock being fractured must be taken into consideration. These properties include: rock/formation permeability, porosity, reservoir pressure, temperature, toughness, and depth. This is usually obtained from well logs, cores, and correlations.

Vishal, Jain, and Singh (2015) showed that the behaviour of rock during different stages of fracturing, fracture propagation, and initiation is unique. The fracture initiates at high breakdown pressure, then with pore pressure the fracture propagates. Over time, if the fracture gets closed with re-fracturing pressure, it re-opens. This highlights the fact that initiation pressure is lower than breakdown pressure. Thus, the fracture will only initiate under breakdown pressure at a point remotely located from the wellbore wall.

Two prominent factors that control the vertical growth of a hydraulic fracture are: the contrast in material properties and the contrast in vertical distribution of in-situ stress (Nasiri, 2015).

The plane of hydraulic fracture is perpendicular to the minimum horizontal in-situ stress, therefore the growth of fracture height is controlled by the vertical distribution of the horizontal minimum in-situ stress. When the contrast of stresses between adjacent stress zones is large, it is expected that the growth of fracture height will be contained (Alqahtani, 2015).

Fracture dimensions are also considered an important factor in hydraulic fracturing for several reasons, of which two are: the incremental increase of injection rates (which are directly dependent on the fracture dimensions), and the possibility of induced fractures growing into unintended zones such as freshwater zones (Al-Obaidi, 2014).

Chapter 3: Methodology

3.1 Modelling Methodology

Because of the nature of the problem, the modelling methodology is broken up into several stages before an actual model is simulated:

1. Characterisation of the Karoo rock as studied from Geel, Schulz, Booth, de Wit, and Horsfield (2013).

2. Once the rock has been characterised, assumptions regarding the zone area of interest in the Karoo are to be made in order to obtain a holistic view. This is based on the availability of the data as seen in Yieldrium (2014).

3. Available data from field scale hydraulic fracturing project/s is obtained, making both direct wellbore observations and indirect field scale observations as performed in the Fort Worth and Appalachian basins in the United States (Yieldrium, 2014).

4. Analysis of data is made, and the published model/s are reviewed.

5. The 2D and P3D models are applied in order to describe the growth of a fracture into its final shape at a particular time, for the fracking process in the Karoo. This is done through a calibration/tuning of the North American shale case/s using Matlab.

The flow chart displayed in Figure 3.1 is a summary of the methodology of the work carried out in this research.

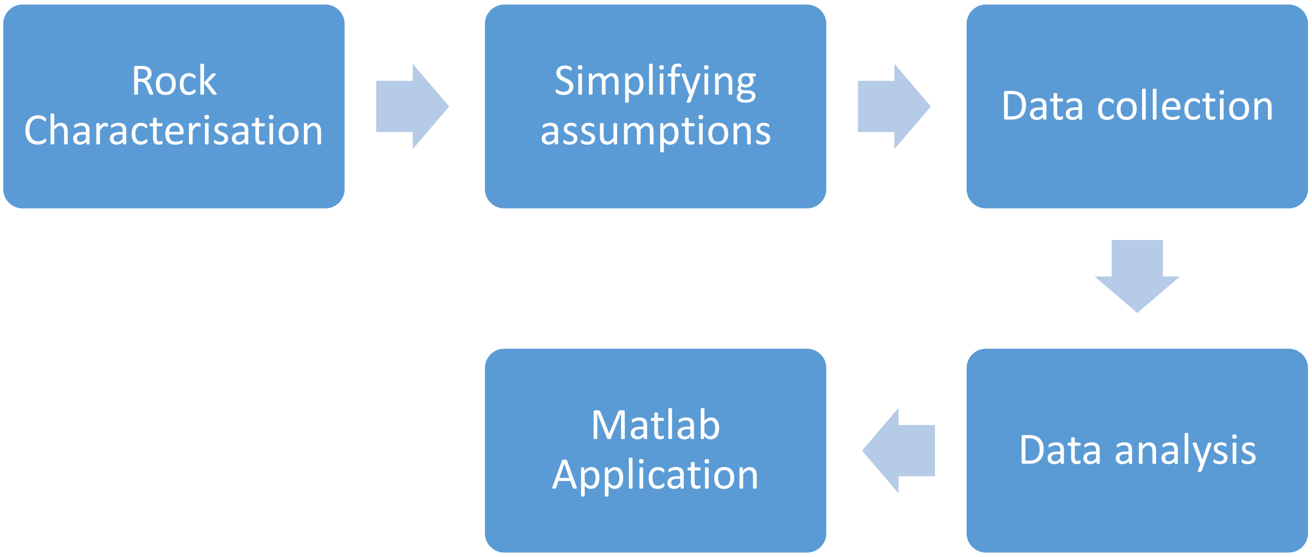

Figure 3. 1: Flow chart summary of the methodology

The designed numerical work that will be used to model the growth of the fracture will provide a means of improved understanding of the process of hydraulic fracturing. It is through hydraulic fracturing design tools that the model can be tested or validated against alternative scenarios.

3.2 Comparison of the Whitehill (SA) with the Marcellus Formation (USA).

Owing to the current political and socio-economic tensions around fracking in South Africa; at this stage, obtaining data sets for fracture treatment design of a well is impossible. Even though there has been some exploratory drilling in the Karoo Basin for analysis of core samples; the lithological logs and profiles produced, considered alone, do not suffice. Because of this, analogous data from formations that resemble those in the Karoo region will be used to build the model. The report conducted by Geel, Schulz, Booth, de Wit, & Horsfield (2013) on the geomechanical and petrophysical properties of shales from the Prince Albert, Whitehill and Collingham formations of the Lower Karoo Supergroup, near Jasenville in the Eastern Cape; revealed a strong potential and candidate selection for these areas to be explored. The Whitehill formation with a total organic carbon (TOC) content averaging 4.5%, fulfils basic prerequisites of successful gas-bearing shales (Decker & Marot, 2012); making it the prime focus for potential shale gas prospects in the Southern Karoo. In order to further corroborate this, an additional comparison was made with the already-exploited shale gas formation in the United States. The results are seen in Table 3.1:

Table 3. 1: The Whitehill shale compared with the Barnett and Marcellus shales. (Bruner and Smosna, 2011, Hoelke J, 2011, Decker and Marot, 2012 and Geel, 2014.)

Formation	**Barnett (Mississippian Shale, Fort Worth Basin, USA)**	**Marcellus (Devonian Shale, Appalachian Basin, USA)**	**Whitehill (Permian Shale, South Eastern Karoo Basin, Greystone area, RSA)**
Mineral (%)			
Quartz	35-50	10-60	13-55
Clays (illite)	10-50	10-35	5-29
Calcite, Dolomite, Siderite	0-30	3-50	3-62
Feldspars	7	0-4	0-24
Pyrite	5	5-13	1-16
Mica	0	5-30	3-22
Porosity (%)	3-6	3-6	2.90 (including Dolomite), 0.83 (excluding dolomite)
Vitrinite reflectance	1.2 (max 1.9)	1.6 (max 3.4)	4
T_{max}	≥465°C	≥475°C	≥573°C
TOC (%)	2-6	1-10	0.7-8.15
Kerogen type	Type II (minor admixture of type III)	Type II (mixture of type III)	Mixture of type II and type III
Estimated size of shale gas play	23 310 km^2	12 499 km^2	155 000 – 183 000 km^2
Formation thickness	107m	15m	~28m
Estimated potential yield	2.5bcf – 40tcf	50 – 900tcf	~32 – 485tcf

Characteristic properties of the Whitehill Formation as a suitable shale gas host compare favourably with those of currently exploited gas fields in the United States. As seen in Table 3.1, the Whitehill formation is rich in organic content, with a Total Organic Content (TOC) averaging 4.4%, and thus fulfils basic prerequisites of gas-bearing shales (Sone & Zoback, 2013) . When looking at the major mineral compositions of shale rock, namely Quartz and Clays (Twine, Jackson, Potgieter, Anderson, & Soobyah, 2012), the Whitehill has an average of 34% and 17% respectively. This compares favourably with the Marcellus, which has averages of 35% and 22% for Quartz and Clays respectively as opposed to the Barnett with 25% and 30%. The Whitehill Formation therefore, in the context of the Karoo Basin, remains an attractive target as a potentially suitable shale gas resource.

3.3 Approximation of Properties as Base Case for the Whitehill Formation

A field case study to obtain detailed lithological, sedimentological, petrographic and geochemical analyses (with particular focus on the black shales of the Whitehill formation) was carried out by Geel, Schulz, Booth, de Wit and Horsfield (2013).-(Geel, Schulz, Booth, de Wit, & Horsfield, 2013). The study site is in the Eastern Cape province, south of Jansenville in the Greystone area.

This area was primarily selected for mapping, core drilling, geochemical and petrological analysis of core samples. Within the selected area, two boreholes were drilled to depths of 100m and 300m respectively. The drilling location was also said to have been strategically chosen: the region where black shales, one of which is the Whitehill formation, was predicted to occur close to the surface.

Another field case study was carried out to estimate the fracture properties and material parameters of a Marcellus shale well based on well logs by using the methodology of petrophysical evaluation of shale gas from Yildrium (2014). The Well region of interest was between 5340 ft (1627.6m) and 5470 ft (1667.3m). A summary of the well properties of the Marcellus shale well is in Table 3.2 :

Table 3. 2: Summary of Marcellus shale well properties (Yildrium, 2014).

Label	Label
Zone of interest	5340 – 5470 ft
Total thickness	130 ft
Well spacing	640 acres
Gas in reservoir	100% Methane
Overburden Stress Gradient	0.96 psi/ft
Average Reservoir Pressure Gradient	0.465
Reservoir Pressure	2483 – 2543 psi
Biot’s Poroelastic Constant	1

Table 3.3 shows the Marcellus Formation geomechanical properties along with those of adjacent formations as calculated from Yildrium (2014). A comparison of the geomechanical properties of Marcellus shale with those of adjacent formations was performed mainly for young's modulus and minimum in-situ stress having effect on fracture height growth to predict future behaviour of hydraulic fracturing strategies.

Table 3. 3:Average calculated mechanical properties of the Marcellus Formation and adjacent formations (Yildrium, 2014).

Rock Formation	Depth (ft)	Poisson's Ratio (v)	Shear Modulus (G) (Mpsi)	Young's Modulus (E) (Mpsi)	Bulk Modulus (K) (Mpsi)	Minimum In-situ Stress (Mpsi)
Stafford Limestone	5200 – 5347	0.248	1.84	4.61	3.10	3360.21
Upper/Lower Marcellus Shale	5347 – 5446	0.213	1.50	3.64	2.13	3244.29
Basal Member	5446 – 5469	0.208	1.66	3.99	2.28	3251.62

From the above properties, a base case for the Whitehill formation in the South Eastern Karoo Basin will be extrapolated and used in subsequent modelling analyses.

Minimum in-situ stress is the most important factor controlling height of fracture in the zone of interest as verified by theoretical, laboratory and field data. The in-situ stress is dependent on other elastic properties such as bulk modulus, shear modulus and Poisson's ratio and tectonic boundary stresses and pore fluid pressure.

Young's modulus is another important controlling factor on height of fracture in the zone of interest besides minimum in-situ stress especially when the net treating pressure is comparable with the in-situ stress contrast.

Minimum in-situ stress and young's modulus contrast at the upper boundary of Marcellus shale is more than those at the lower boundary so that upper boundary of Marcellus shale would act as a barrier to hinder fracture growth when stimulation treatments are applied (Yildrium, 2014). This effect is thus also expected to be prevalent for Whitehill shale.

Also, as expected from basic rock physics principles, the elastic properties of these shale rocks are a strong function of their material composition (Sone & Zoback, 2013) . However, the true shape of the fracture in the Karoo will only really be revealed by having the exact strength and stress of the rock.

The growth of a fracture can be stopped in cases where there is a relatively higher or lower Young's modulus at the adjacent formations. The necessary data to be used as input into the PKN, KGD and P3D models is seen in Table 3.4.

Table 3. 4: Fracture properties and Material parameters

Label	
Shear Modulus	$G = 1.466 \times 10^6$ psi
Drained Poisson's ratio	$v = 0.2$
Fluid Viscosity	$\mu = 1$ cp
In-situ stress	$\sigma_{min} = 3200$ psi
Pumping rate	$Q = 62.5$ bbl/min
Wellbore radius	$r_w = 0.2$ft
Passed time	$t_{f} =$ 0.3 min

All models must be run with the same inputs in order to compare the models in a reasonable sense.

Chapter 4: Fracture growth and prediction Results

4.1 KGD model

Figures 4.1 – 4.4 show the fracture growth and prediction of the final shape for the constant height KGD model. Code used to generate the figures can be found in Appendix B2.

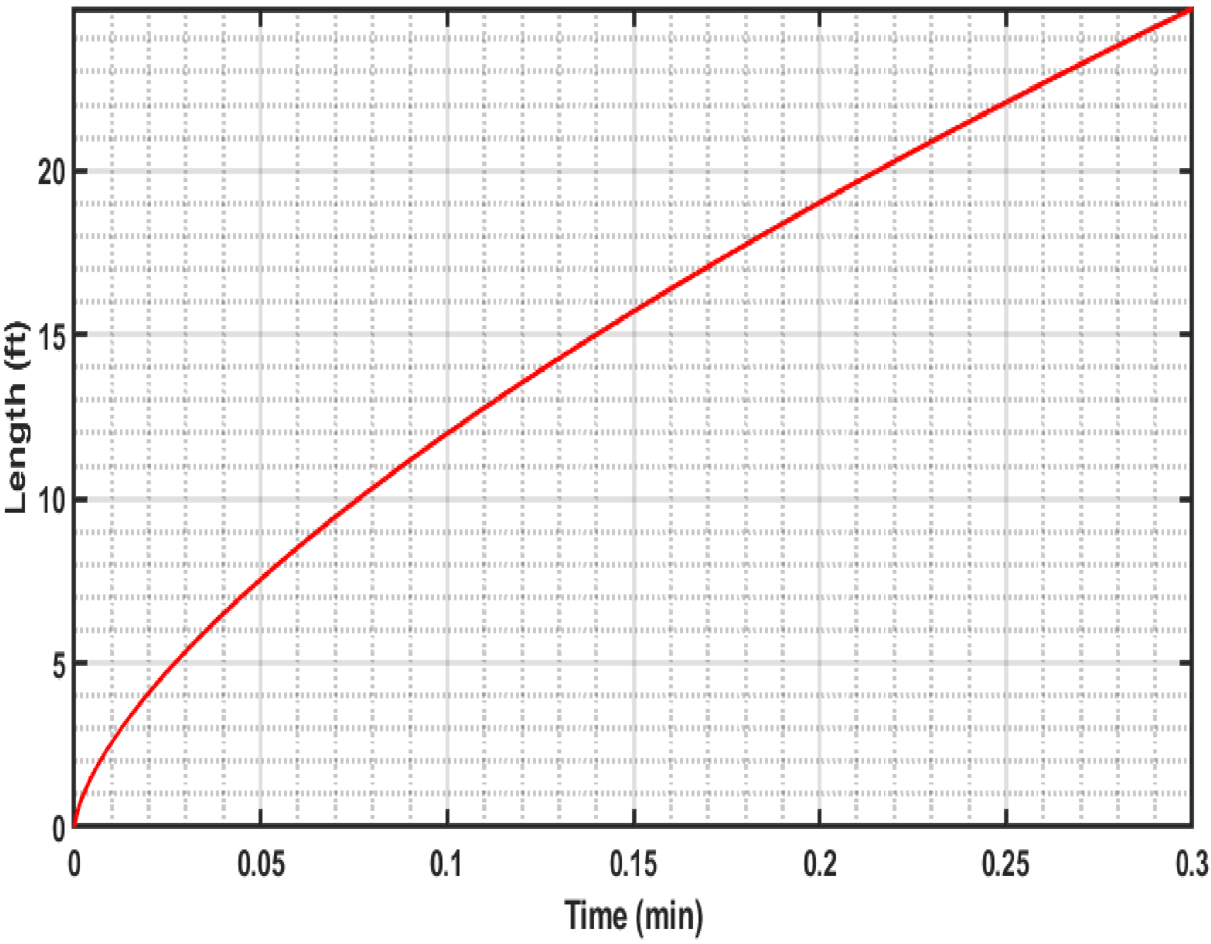

Figure 4. 1: Fracture length vs time for KGD model.

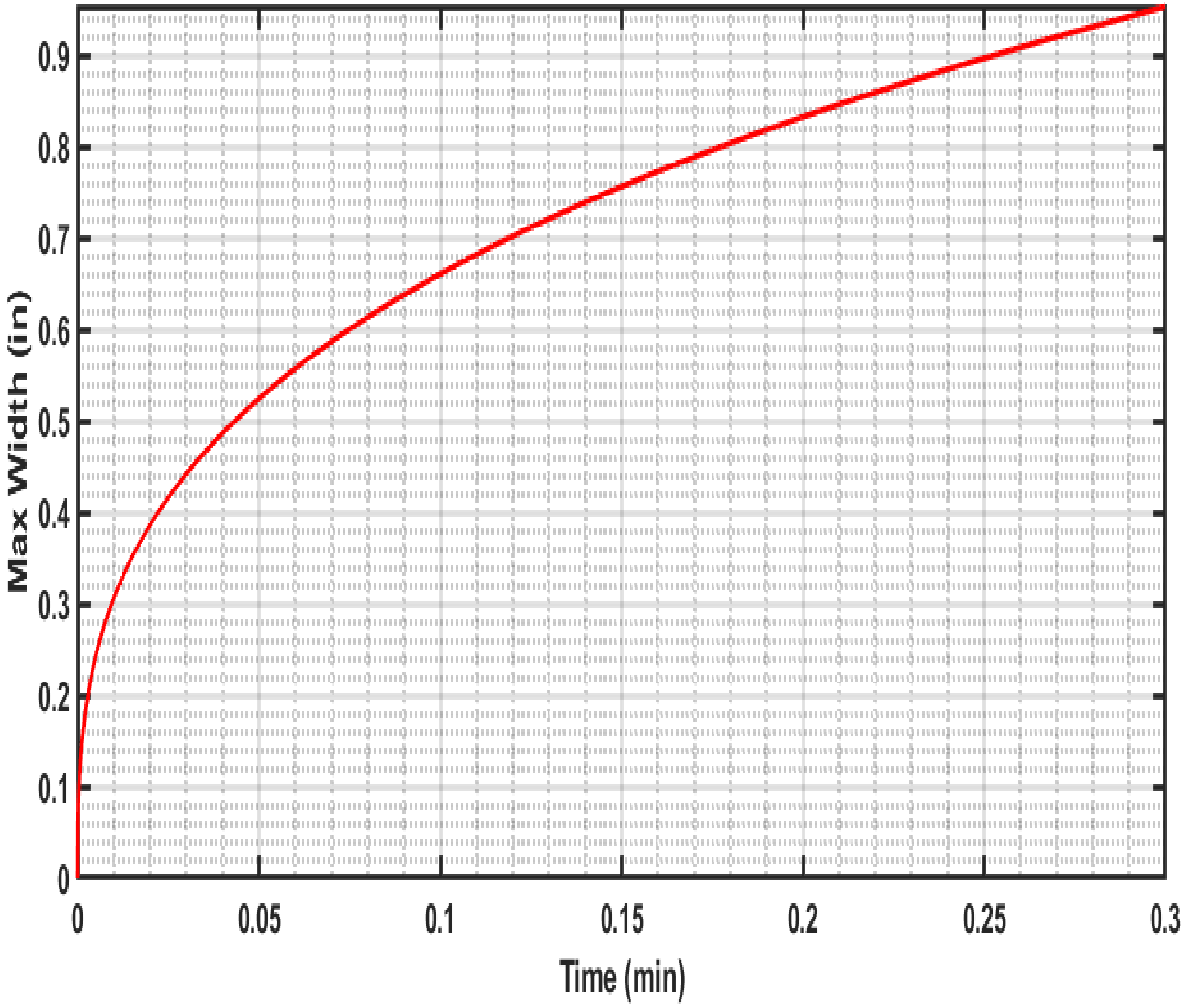

Figure 4. 2: Maximum fracture width vs time for KGD model.

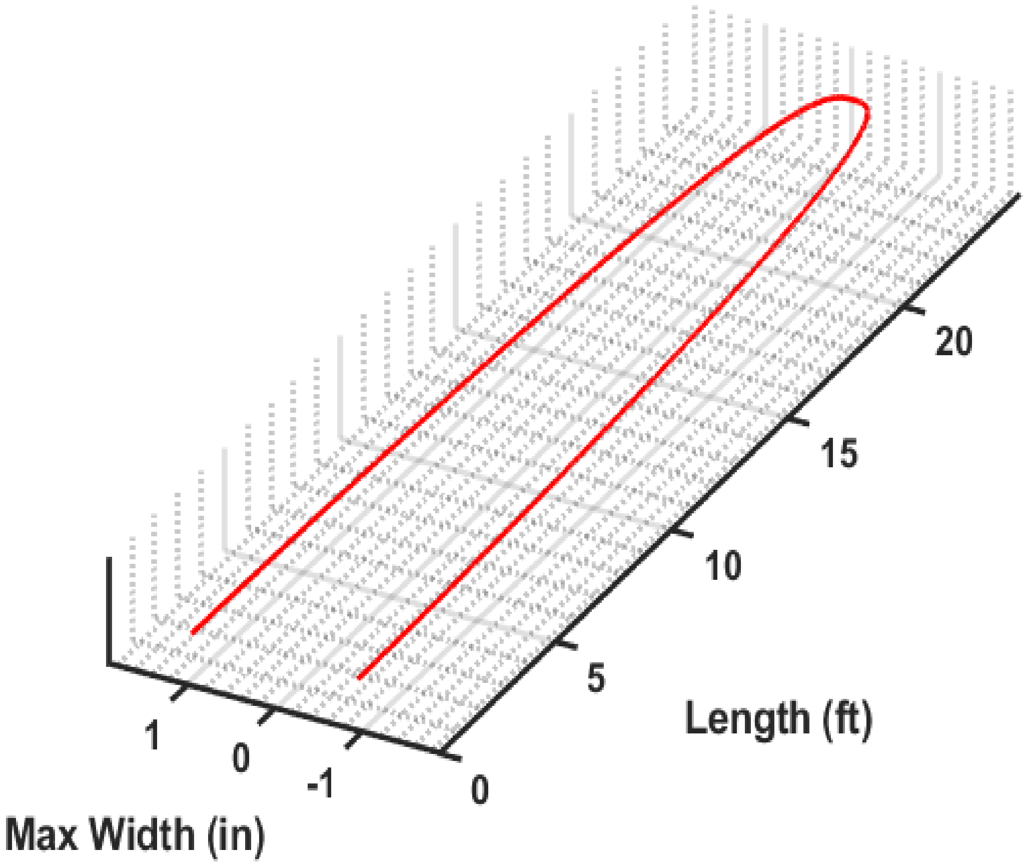

Figure 4. 3: Fracture length vs Maximum width for KGD model.

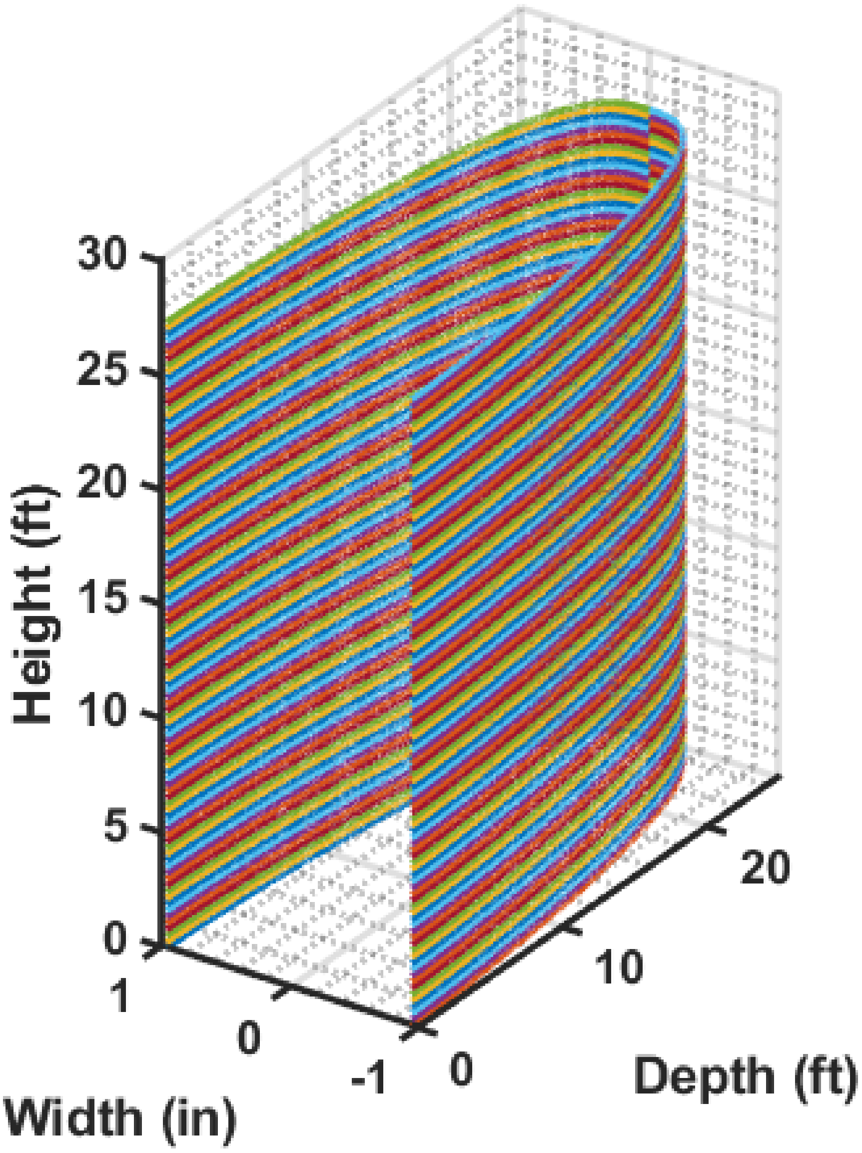

Figure 4. 4: 3D prediction of the fracture for KGD model.

4.2 PKN model

Figures 4.5 – 4.9 show the fracture growth and prediction of the final shape for the constant height PKN model. Code used to generate the figures can be found in Appendix B3.

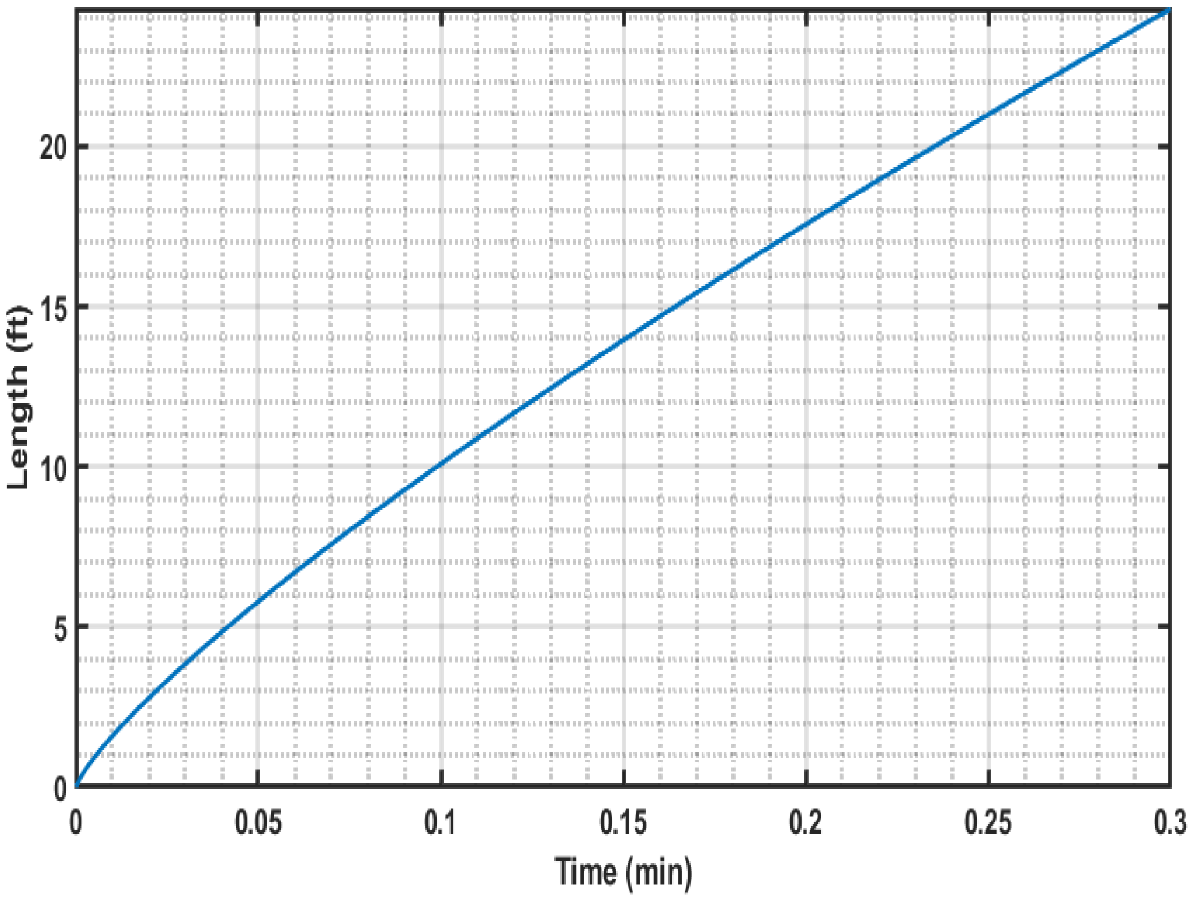

Figure 4. 5: Fracture length vs time for PKN model

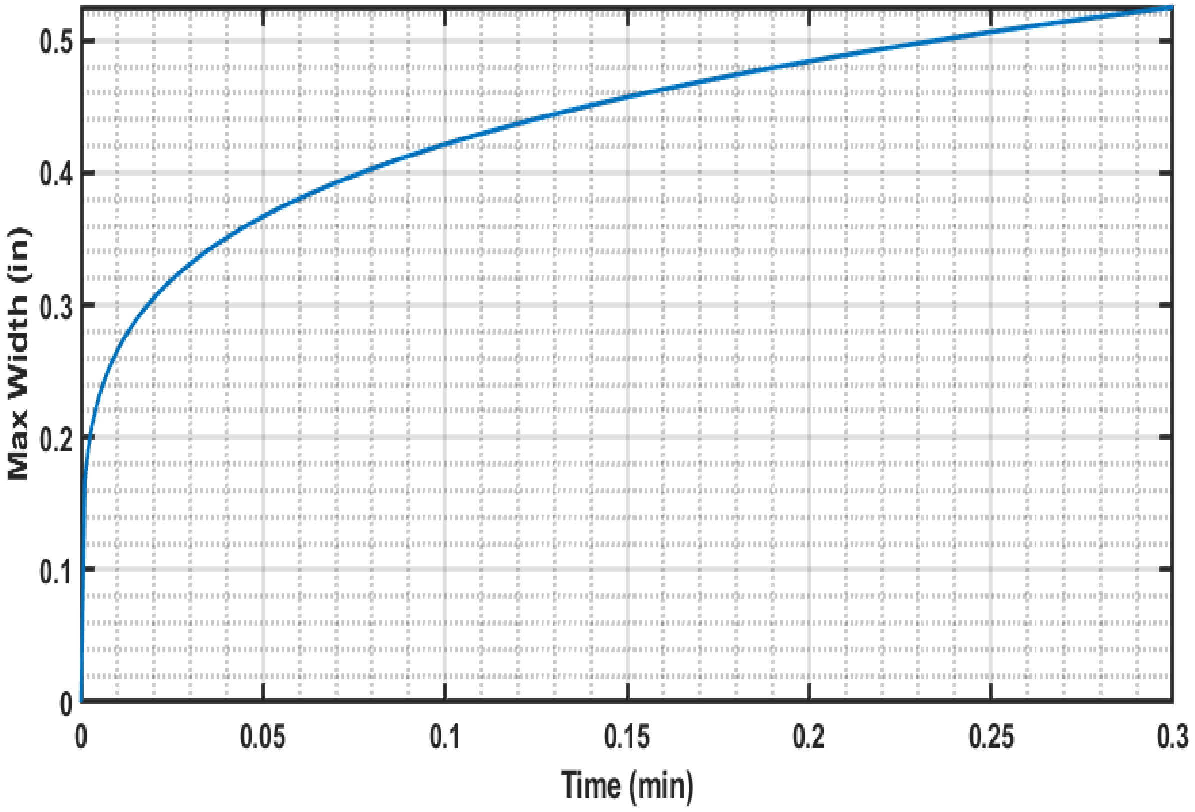

Figure 4. 6:Maximum fracture width vs time for PKN model.

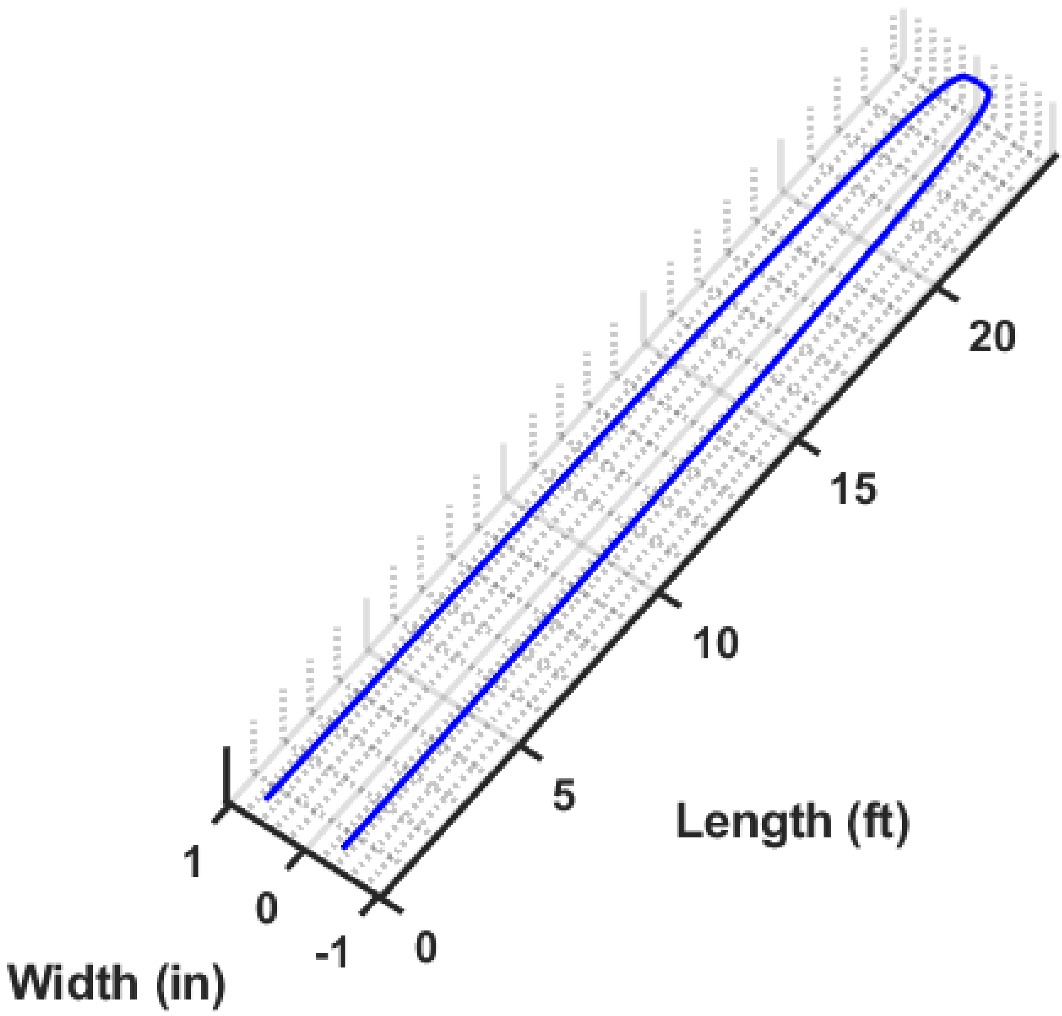

Figure 4. 7: Fracture width vs length for PKN model.

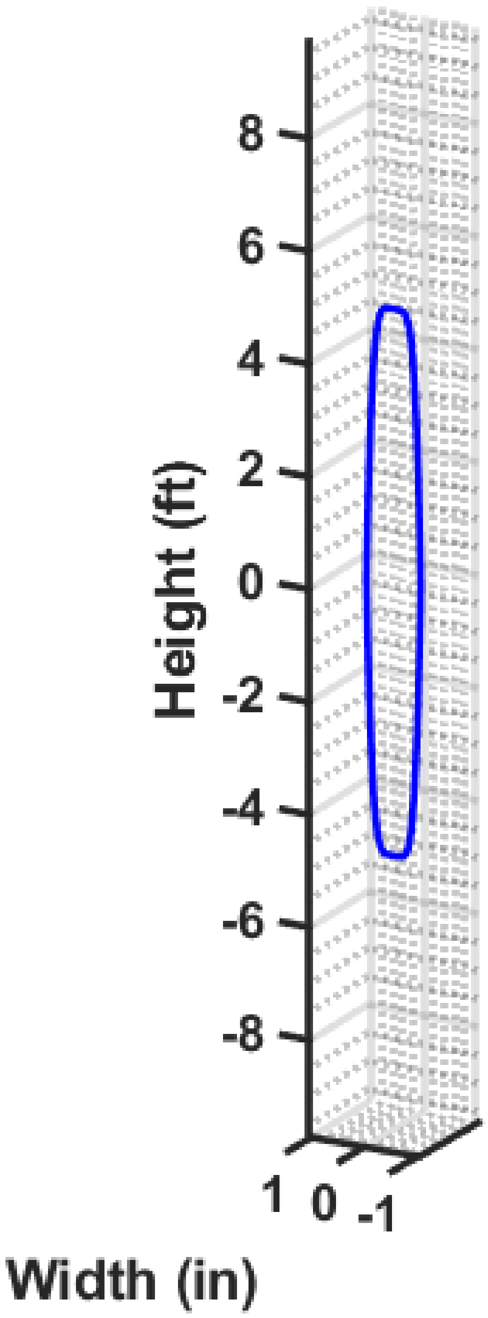

Figure 4. 8: Fracture width vs height (in the z-y plane)

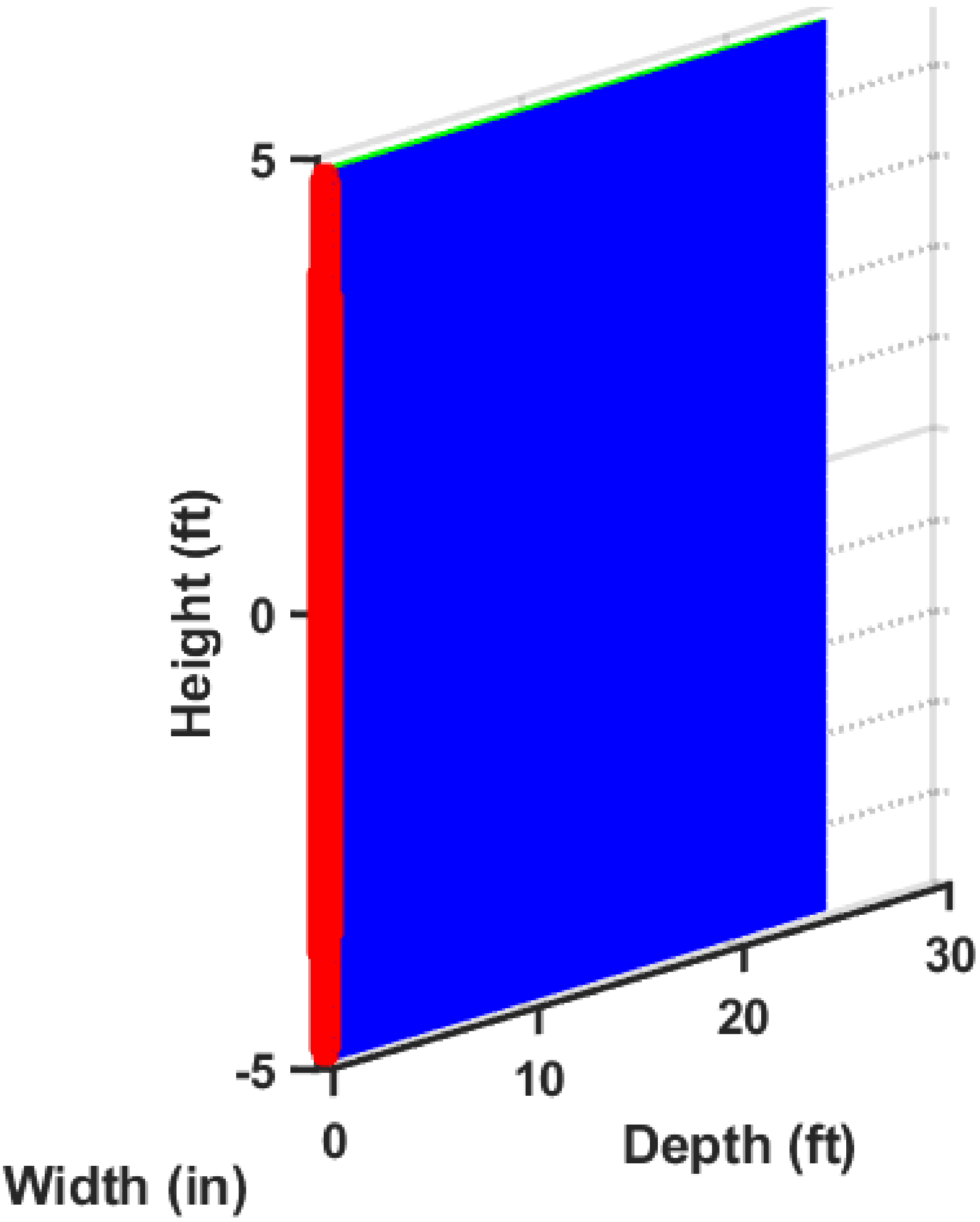

Figure 4. 9: 3D prediction of fracture for PKN model.

4.3 P3D model

Figures 4.10 – 4.12 show the fracture growth and prediction of the final shape for the P3D model. Code used to generate the figures can be found in Appendix B4.

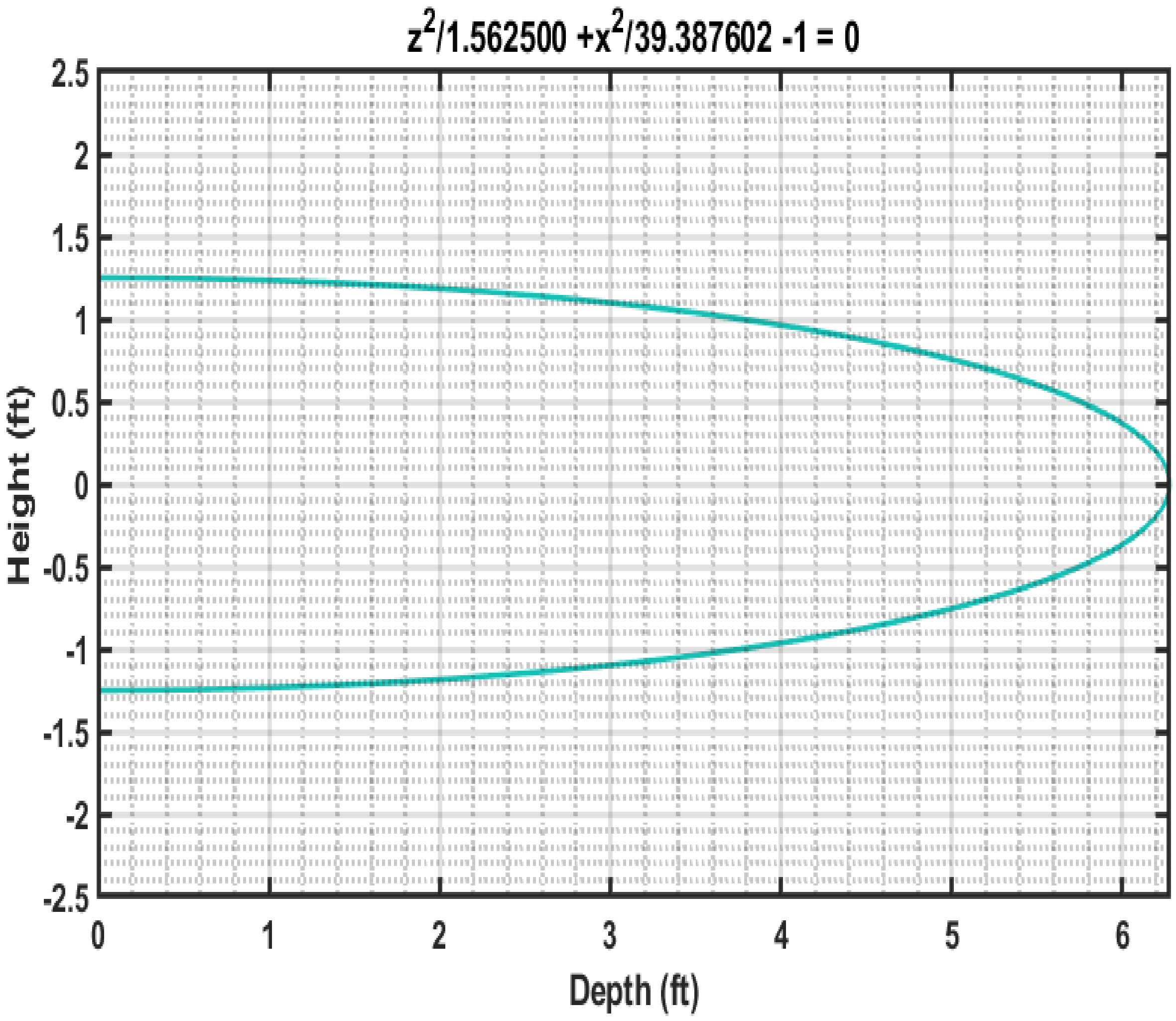

Figure 4. 10: Fracture height vs depth for P3D model

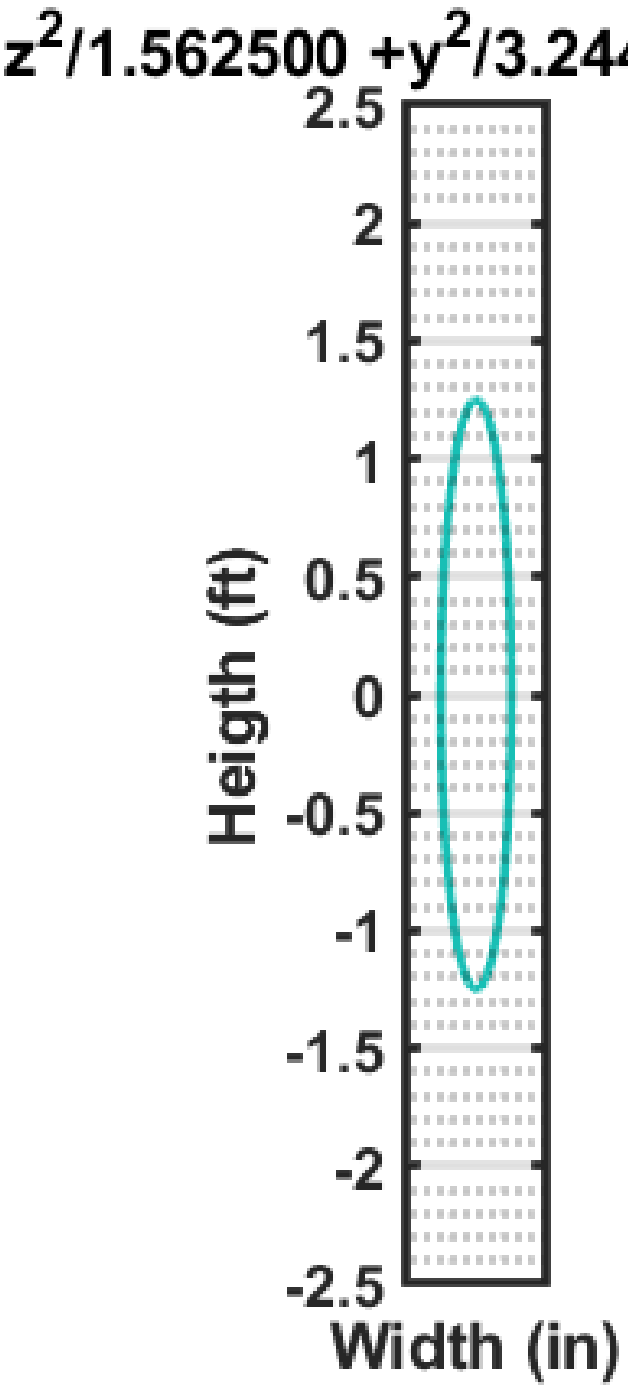

Figure 4. 11: Fracture height vs width for P3D model.

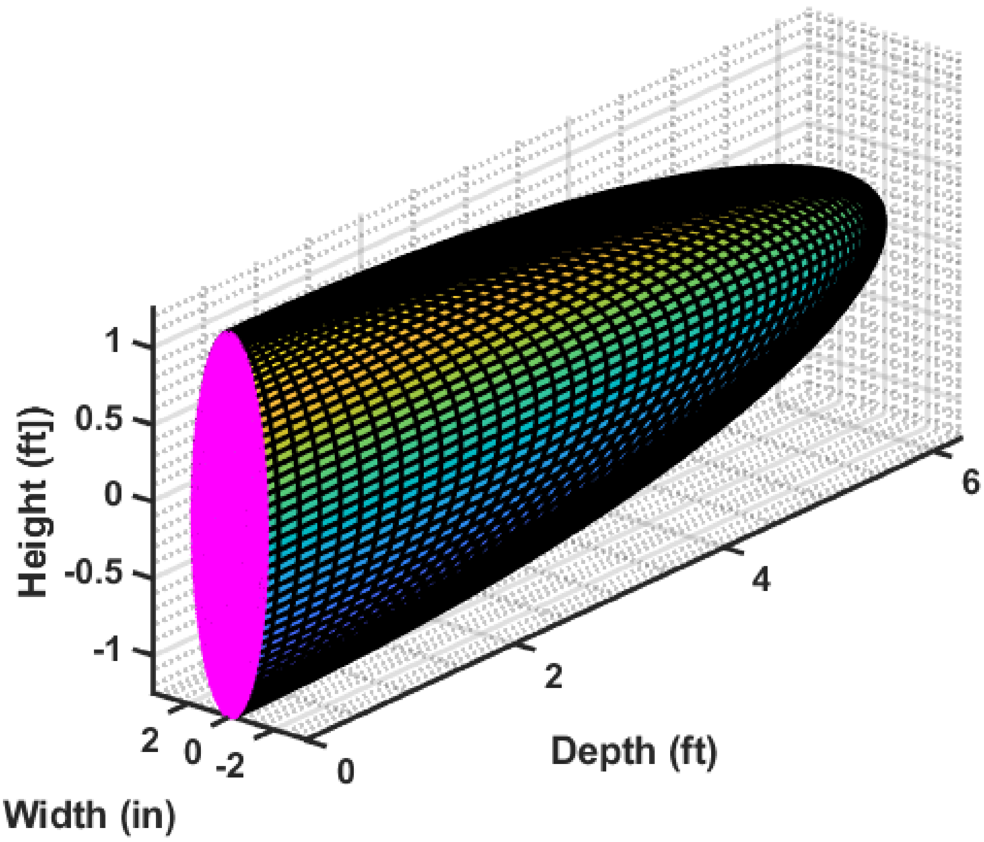

Figure 4. 12: Prediction of fracture shape for the P3D model.

4.4 Pressure behaviour with time

Figures 4.13 – 4.15 show the pressure changes vs time for all three models. Matlab code used to generate the models can be found in Appendix B1.

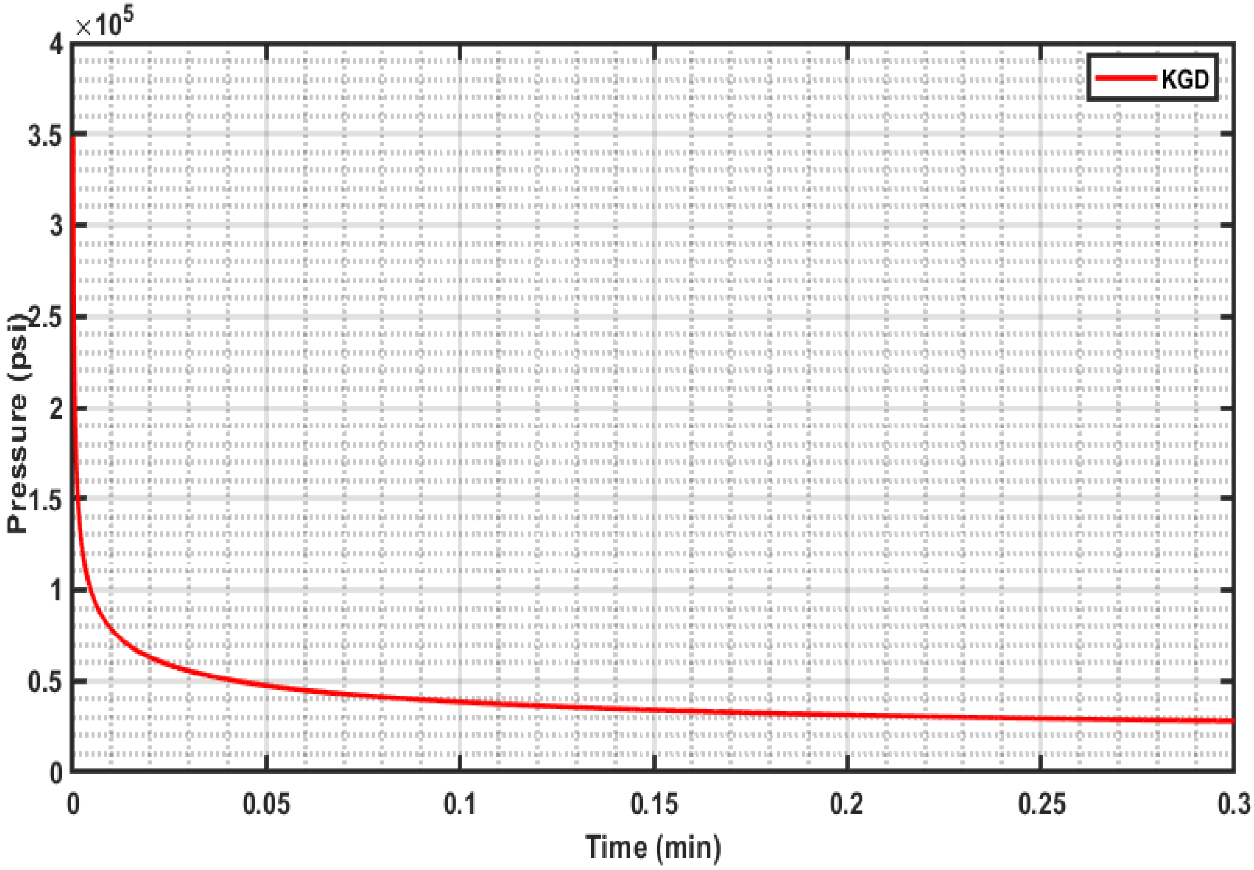

Figure 4. 13: Pressure change vs time for KGD model.

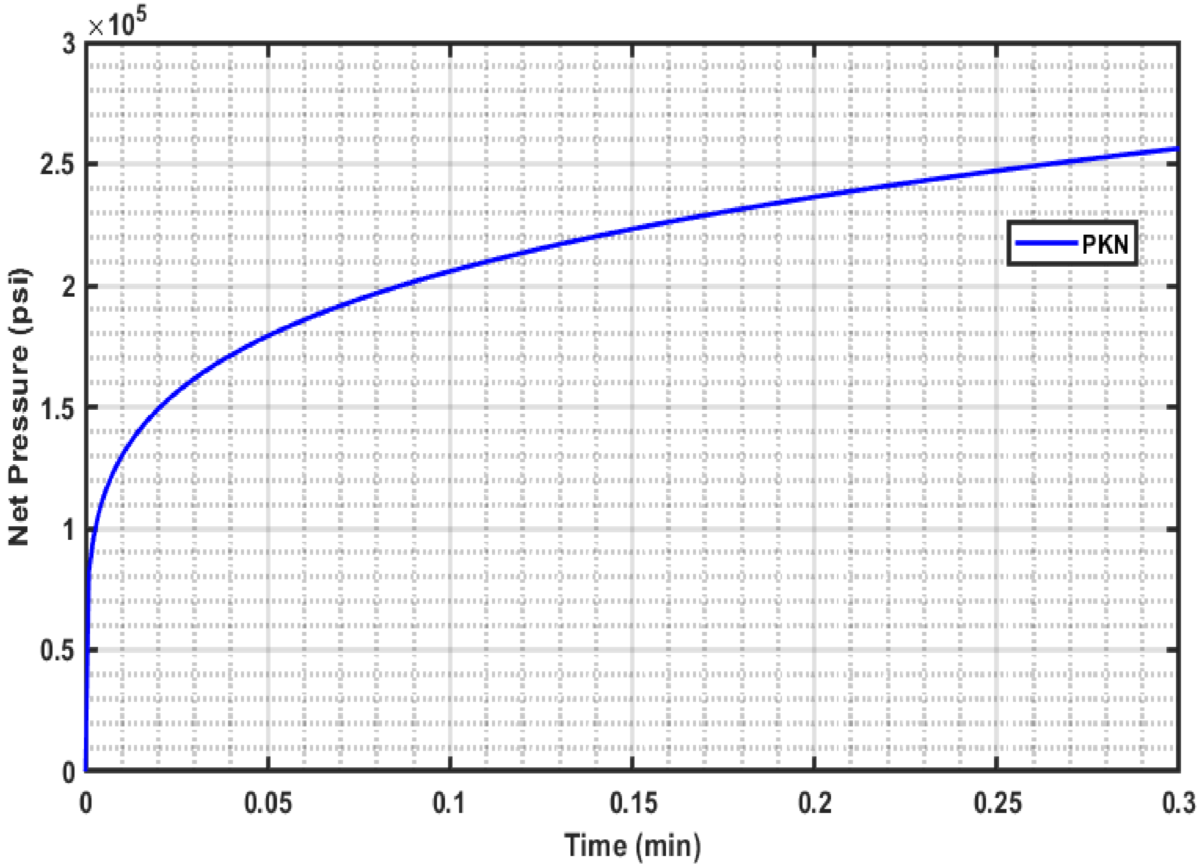

Figure 4. 14: Pressure change vs time for PKN model.

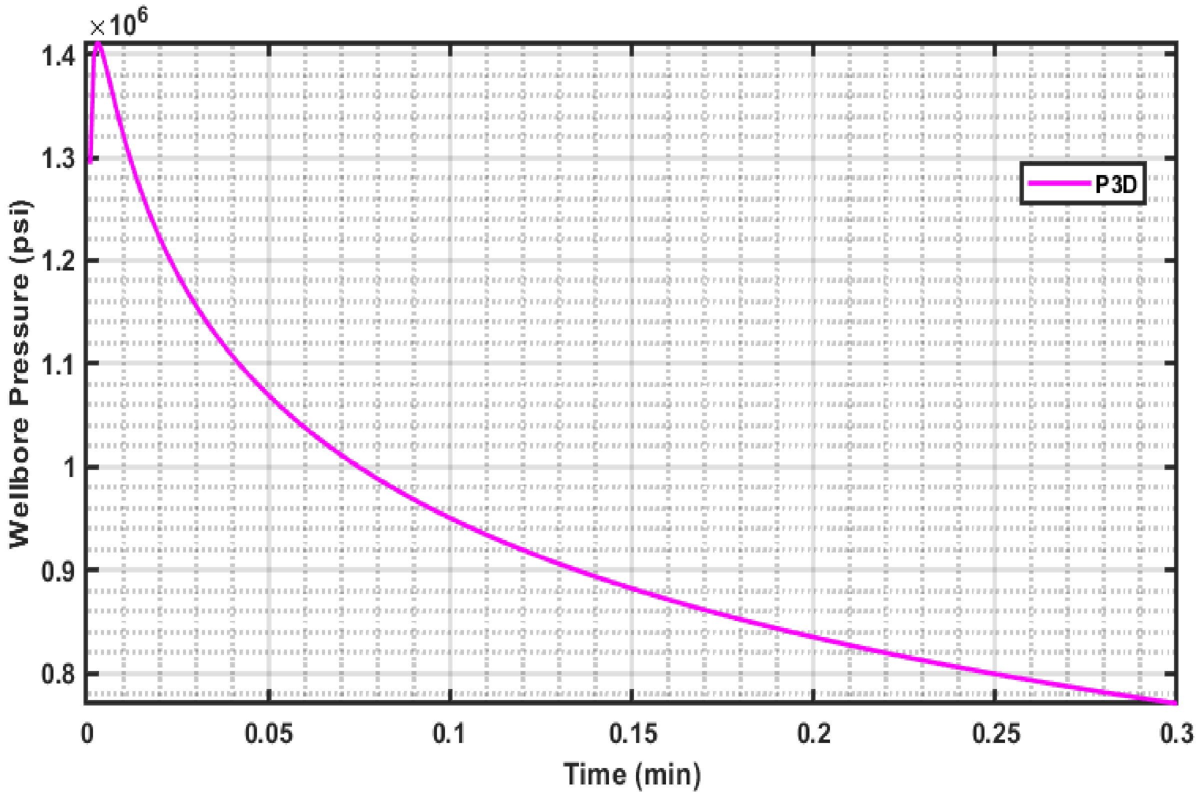

Figure 4. 15: Pressure change vs time for P3D model.

Chapter 5: Analysis and Discussion

Upon the initiation of pumping, there is a gradual increase in fluid-pressure immediately surrounding the injection site. Both within the impermeable, intact rock matrix and pre-existing rock mass fractures. When the injection pressure exceeds the rock strength, new fractures begin to propagate away from the injection point (in a direction perpendicular to the least principal stress; i.e. parallel to the maximum principal stress). As injection continues, a complex interaction between new and pre-existing fractures emerges as a characteristic of the coupled hydro-mechanical simulation.

Newly formed fractures tend to terminate when they encounter pre-existing fractures as fluid flow is diverted along these highly permeable pathways. Ultimately, the shape and extent of the stimulated volume which accounts for the influence of rock-mass fabric on the hydraulic fracture process, is obtained. The simulated fracture network and its hydraulic parameters can be easily exported for further processing or use as unique input for production analysis.

In the development of the PKN and KGD models for hydraulic fracturing, it was stated by Zhao, Li, Zhu, & Ru (2018), that the average net pressure in the fracture would greatly exceed the minimum pressure for propagation, unless the fluid flow injection rate was extremely small or the fluid had an unrealistically low viscosity. Therefore, under typical fracturing conditions, the pressure resulting from fluid injection is practically larger than the minimum pressure (breakdown pressure) required creating or extending a stationary fracture. This justifies neglecting fracture mechanics effects in the models. Furthermore, it was stated that the fracture would continue to extend after pumping stopped, until either leak-off affects further extension or the minimum pressure for fracture propagation is reached (Smith & Shlyapobersky, 2014).

Figure 4.1 shows that the length of the fracture increases with a higher rate than the fracture width in Figure 4.2 which increases in proportion to $t^{1/3}$. After 22 seconds of fracture growth, the ratio of the final L/W equals 285, indicates a sharp curvy tip, as seen in Figure 4.3 which in turn approves the low effect of the tip geometry on fracture growth in this model (Gerrtsma & De Klerk, 1969). Geertsma and de Klerk (1969) argue that since the tip is a local singularity of the fracture, its effect on the overall fracture geometry should be small and their solution is a good approximation for the fracture opening width and the overall fracture length.

What is observed in Figures 4.1 - 4.3 can be true for Figures 4.5 – 4.7 to some extent too. Although the underlying mechanics in the KGD and PKN models differ significantly, under similar assumptions (no leak off) they yield similar results, however their difference in predicted opening widths cannot be neglected.

Looking at Figures 4.4 and 4.9, there is an inconsistency in the final predicted 3D shapes for the two models. The y-z plane in Figure 4.4 is rectangular which means that the 3D surface is an extension of the x-y plane diagram into the 3D space. The 3D surface in Figure 4.9, however, follows a semi-parabola shape in the x-y place and a semi-ellipse in the y-z place. Every cross-section perpendicular to the x-axis cuts the surface in the semi-ellipse: (L(time), W(time), H). Looking at the general equation of an ellipse, $\frac{Z^2}{a^2} + \frac{y^2}{b^2} = 1$, it is important to note that it has a changing constant variable b (and a, if height is not constant) at any moment. This means that the growth of a fracture in a specific period, even in its simplest form, does not obey a simple mathematical equation.

However, the modified P3D model eventually predicts a complete ellipsoid in 3D space at a specific time which can be seen in the Figure 4.12.

Initially, the difference between the prediction of pressure by the two 2D models in Figures 4.13 and 4.14 is noticeable, however, as time progresses, the difference reaches a constant maximum. The pressure predicted by the KGD model in Figure 4.13 declines from 3.633×10^5 to 3.466×10^4 psi. Whereas the pressure of the PKN model in Figure 4.14 increases to 2.564×10^5 psi. The pressure of the P3D model in Figure 4.15 increases to a peak of 1.411×10^6 psi at t = 0.24sec before declining to a final 7.709×10^5 psi. The wellbore pressure predicted by the PKN model, in contrast to the KGD model, rises as the fracture length increases. However, the pressure predicted by the KGD model approaches the in-situ stress σ_{min} for a large value of L.

Chapter 6: Conclusions and Recommendations

6.1 Conclusions

This work analyses the mechanisms of hydraulic fracturing of shale gas. A comparison between Barnett and Marcellus shale with the Whitehill shale was done. Characteristic properties of the Whitehill formation was looked at for suitable comparison with the existing exploitation. Owing to a lack of field data from the Karoo, the growth of a fracture for analogous, Marcelus shale rock was modelled using well-known 2D and 3D models of hydraulic fracturing. The methodical approach was explained before the MATLAB simulation in order to investigate the fracture growth models.

The wellbore pressure predicted by the PKN model rises as the fracture length increases. and the KGD model approaches the in-situ stress σmin for a large value of L. The modified P3D model predicts a complete ellipsoid in 3D space at a specific time. The comparisons show that the differences in calculated fracture lengths can be large, despite the similarities in the models. For the same input parameters, the fracture geometries calculated by each of these models differ widely. Although solutions to the models were found, the findings lack validation of the data with field data.

Understanding the mechanisms of fracking in a complex geological setting is the first step in testing the viability of the procedure. This work sought to understand how fracturing would commence in a complex environment as the Karoo. Given the different vantage points each model provides, there is sufficient information that suggests the viability of hydraulic fracturing in the Karoo.

6.2 Recommendations

Though this study addressed certain problems and questions pertaining to hydraulic fracturing modelling specifically in the Karoo region, there is still room for improvement. In order to improve future models for this technique further questions need to be addressed. Based in this study the following aspects could be taken into consideration:

- 2D and 3D Models to be validated with field data.
- Each model can be used to research fracture propagation.
- Accurate data to be used to show the likelihood of fractures extending upwards into shallow basins.

- Taking formation temperature into account in future modelling.
- Use of real-time, various hydraulic fracturing programs.
- It would also be beneficial to perform this same type of study for different input conditions. This case was chosen because it was a realistic field situation for which detailed data were available. Other warranted cases are those where there are minimal stress contrasts and where the stress contrasts are extremely large.

References

Abuaisha, M., Eaton, D., Priest, J., & Wong, R. (n.d.). Simulating hydraulic fracturing using Finite – Discrete Element Method (FDEM): Effects of pre – existing joints and induced seismicity. *Microseismic Industry consortium, 6*, pp. 63-80.

Adachi, J. I., Detournay, E., & Peirce, A. P. (2010). Analysis of the classical pseudo-3D model for hydraulic fracture with equilibrium height across stress barriers. *International journal of rock mechanics and mining sciences, 47*(4), 625-639. doi:https://doi.org/10.1016/j.ijrmms.2010.03.008

Adachi, J., Siebritis, B., Peirce, A., & Desroches, J. (2007, July). Computer simulation of hydraulic fractures. *International Journal of Rock Mechanics and Mining Sciences, 44*, 739-757. doi:https://doi.org/10.1016/j.ijrmms.2006.11.006

Alqahtani, N. B. (2015). *Experimental Study and Finite Element Modelling of Cryogenic Fracturing in Unconventional Reservoirs.* PhD Thesis, Colarado School of Mines, Department of Petroleum Engineering. Retrieved Novemeber 24, 2017, from https://dspace.library.colostate.edu/handle/11124/20319

Barenblatt, G. I. (1962). The Mathematical Theory of Equilibrium Cracks in Brittle Fracture. *Advances in Applied Mechanics, 7,* 55-129. doi:https://doi.org/10.1016/S0065-2156(08)70121-2

Bischof-Niemz, T. (2017). *What could South Africa's Energy Future look like?* CSIR. Retrieved April 2017, from https://90by2030.org.za/wp-content/uploads/2017/05/Energy-Scenarios-for-RSA-CSIR-Tobias-Bischof-Niemz.pdf

Brookes, B. W., Cohen, S. D., Morris, J., & Orme-Zavaleta, J. (2014, April 4). The role of toxicological science in meeting the challenges and opportunities of hydraulic fracturing. *Toxicological Sciences*. doi:10.1093/toxsci/kfu-61

Dandekar, A. Y. (2013). Formation of petroleum reservoirs. In A. Y. Dandekar, *Petroleum Reservoir Rock and Fluid Propoerties* (2nd ed., pp. 1-4). CRC Press.

DBSA. (2014). *Fracking in South Africa: In search of a strategy for the DBSA.* Midrand: DBSA. Retrieved July 2017, from https://www.dbsa.org/EN/About-Us/Publications/Documents/Concept%20Note%20Fracking%20in%20South%20Africa%20-%20A%20proposed%20strategy%20for%20DBSA%20-%20March%202014.pdf

Decker, J., & Marot, J. (2012). *Investigation of hydraulic fracturing in the Karoo South Africa. Annexture A: Resource assessment.* Petroleum Agency South Africa. Retrieved July 2017, from http://www.dmr.gov.za/publications/viewdownload/182/854.html

Desroches, J., & Bratton, T. (2000). Properties related to the deformation and fracturing of rock. In M. J. Economides, & K. G. Nolte, *Reservoir Stimulation* (pp. 13-15). John Wiley & Sons.

England, A. H., & Green, A. E. (1963, April). Some two-dimensional punch and crack problems in classical elasticity. *Mathematical Proceedings of the Cambridge Philosophical Society, 59*(2), 489-500. doi:doi:10.1017/S0305004100037099

Fakir, S. (2015). *Framework to assess the economic reality of shale gas in South Africa.* WWF.

Frink, J. (2013). *Hydraulic Fracturing Chemicals And Fluids Technology* (1st ed.). Amsterdam: Gulf Professional Publishing. Retrieved April 11, 2017, from http://0-web.b.ebscohost.com.innopac.wits.ac.za/ehost/detail/detail/bmxlYmtfXzU0Mzc0N19fQU41?sid=d7c90fca-c733-4eb9-90b8-42b4b0b1193e@sessionmgr101&vid=0#AN=543747&db=nlebk

Geel, C., Schulz, H., Booth, P., de Wit, M., & Horsfield, B. (2013). Shale gas characteristics of Permian black shales in South Africa: results from recent drilling in the Ecca Group (Eastern Cape). *Energy Procadia, 40*, 256-265. doi:10.1016/j.egypro.2013.08.030

Gerrtsma, J., & De Klerk, F. (1969). A rapid method of predicting width and extent of hydraulically induced fractures. *Journal of Petroleum Technology, 21*(12). doi:https://doi.org/10.2118/2458-PA

Gidley, J. L., Holditch, S. A., Nierde, D. E., & Veatch, R. N. (1989). *Two-dimensional fracture propagation models.* (J. L. Gidley, Ed.) Richardson, Texas, United States of America: Society of Petroleum Engineers. Retrieved August 2017

Hattori, G., Trevelyan, J., Augarde, C., Coombs, W., & Aplin, A. (2017). Numerical Simulation of Fracturing in Shale Rocks: Current state and future approached=s. *Archives of Computational methods in Engineering, 24*(2), 281-387.

Hoeven, J. A. (2017). *An investigation into the effects of anisotropy and heterogeneity of fracture permeability on flow and thermal transport.* Master Thesis, Utrecht University, Faculty of Geosciences. Retrieved October 2017, from https://dspace.library.uu.nl/handle/1874/349778

Howard, C. C., & Fast, C. R. (1957). Optimum fluid characteristics for fracture extension. *API Drilling and Production Practice, 24*(261).

Howard, G. C., & Fast, C. R. (1970). *Hydraulic Fracturing* (Vol. II). New York: American Institute of Mining, Metallurgical and Petroleum Engineers.

Khristianovic, S. A., & Zheltov, Y. P. (1955). Formation of Vertical Fractures by Means of Highly Viscous Liquid. *Forth World Petroleum Congress*, (pp. 579 - 586). Rome. Retrieved August 2018

Kovalyshen, Y., & Detournay, E. (2009, January). A Reexamination of the classical PKN model of Hyrdaulic Fracture. *Transport in Porous Media, 2*(81), 317-339. doi:10.1007/s11242-009-9403-4

Li, Q., Xing, H., Liu, J., & Liu, X. (2015, March 3). A review on hydraulic fracturing of unconventional reservoir. *Petroleum, 1*(1), 8-15. Retrieved May 25, 2017, from http://www.sciencedirect.com/science/article/pii/S2405656115000140

Linkov, A. M. (2014). *Solution of Hydraulic Fracture Problem Accounting for Lag.* Rzeszow University of Technology, Institute for Problems of Mechanical Engineering, Saint Petersburg. Retrieved September 2017, from https://arxiv.org/ftp/arxiv/papers/1404/1404.5246

Morales, R. H., & Abou-Sayed, A. S. (1989, February). Microcomputer analysis of hydraulic fracture behavior with a pseudo-three dimensional simulator. *SPE Production Engineering, I*(4), 69-74. doi:10.2118/15305-PA

Motiang, M., & Nembahe, R. (2017). *Energy Price Report.* Pretoria: Department of Energy: Republic of South Africa. Retrieved August 2017, from http://www.energy.gov.za/files/media/explained/Energy-Price-Report-2017.pdf

Nasiri, A. (2015). *A Comparison Study of KGD, PKN and a Modified P3D Model.* International Campus of Sheriff University of Technology. Researchgate. Retrieved August 2017, from https://www.researchgate.net/publication/280568163

Nell, L. (2017, September). *News Article: Don't Frack with our Karoo.* Retrieved from Oudtshoorn Courant: https://www.oudtshoorncourant.com/News/Article/General/don-t-frack-with-our-karoo-20170711

Nguyen, V. P. (2016). *Computational modeling of hydraulic fracture: state of the art, theory, implementation and benchmark tests.* Monash UNiversity. Research Gate. doi:10.13140/RG.2.1.2840.5521

Nolen-Hoeksema, R. (2013). Elements of Hydraulic Fracturing. *Oilfield Review,* 51-52. Retrieved May 2017, from https://www.researchgate.net/publication/291020885_Elements_of_hydraulic_fracturing

Nordgren, R. P. (1972, August). Propagation of a vertical hydraulic fracture. *Society of Petroleum engineers journal, 12*(04), 306-314. doi:https://doi.org/10.2118/3009-PA

Nordgren, R. P. (1972, August). Propagation of a Vertical Hydraulic Fracture. *12*(4). doi:https://doi.org/10.2118/3009-PA

O'Connor, C., de Lange, S., de Nagy Koves Hrabar, S., Mauter, M., Shand, M., & Xiphu, M. (2016). *South Africa's technical readiness to support the shale gas industry*. Pretoria: Academy of Science of South Africa. doi:http://dx.doi.org/10.17159/assaf.2016/0003

Perkins, T. K., & Kern, L. R. (1961, September). Widths of Hydraulic Fractures. *Journal of Petroluem Technology, 13*(09). doi:10.2118/89-PA

PWC. (2012, June). *Industries: Oil, Gas and energy*. Retrieved April 04, 2017, from Price Waterhouse Coopers: https://www.pwc.co.za/en/assets/pdf/the-gas-equation-june-2012.pdf

Rahman, M. M., & Rahman, M. K. (2010). A review of hydraulic fracture models and development of an improved pseudo-3D model for stimulating tight oil/gas sand. *Energy Sources, 32*, 1416-1436. doi:10.1080/15567030903060523

Research, E. I. (2017, August). *Finance: articles.* Retrieved from Deloitte South Africa: https://www2.deloitte.com/za/en/pages/finance/articles/a-fracking-boost-for-the-south-african-economy.html#

Schilizzi, R. (2004). The Square Killometer Array. *Proceedings SPIE. 5489*, p. 62. Kona: Ground-based Telescope. doi:10.1117/12.551206

Smith, M. B., & Shlyapobersky, J. W. (2014). Basics of Hydraulic Fracturing. In M. J. Economides, & K. G. Nolte, *Reservoir Stimulation* (pp. 139-189). Wiley.

Sone, H., & Zoback, M. D. (2013). Mechanical properties of shale-gas reservoir rocks — Part 1: Static and dynamic elastic properties and anisotropy. *Geophysics, 78*(5), 381-392. doi:10.1190/GEO2013-0050.1

Twine, T., Jackson, M., Potgieter, R., Anderson, D., & Soobyah, L. (2012). *KAROO SHALE GAS REPORT: SPECIAL REPORT ON ECONOMIC CONSIDERATIONS SURROUNDING POTENTIAL SHALE GAS RESOURCES IN THE SOUTHERN KAROO OF SOUTH AFRICA.* Econometrix (Pty) Ltd.

Vishal, V., Jain, N., & Singh, T. (2015). Three dimensional modelling of propagation of hydraulic fractures in shale at different injection pressures. *Sustainable Environment Research, 25*(4), 217-225.

Vishal, V., Jain, N., & Singh, T. N. (2015, July 11). Three dimensional modeling of propagation of hydraulic fractures in shale at different injection pressures. *Sustainable environment research, IV*(25), 217-225. Retrieved May 28, 2017, from https://www.researchgate.net/publication/279925299

Wang, Y., Li, X., & Tang, C. A. (2016, May 26). Effect of injection rate on hydraulic fracturing in naturally fractured shale formations: a numerical study. *Environmental Earth Science, 75*, 935-951. doi:10.1007/s12665-016-5308-z

Wangen, M. (2013). Finite element modeling of hydraulic fracturing in 3D. *Computational Geosciences, 17*(4), 647-659.

Wangen, M. (2017, April 1). A 2D volume conservative numerical model of hydraulic fracturing. *Computers and Structures, 182*, 448-458. doi:https://doi.org/10.1016/j.compstruc.2017.01.003

Warpinski, N. (2011). *Fracture Growth in Layered and Discontinued Media.* Pinnacle Halliburton. Retrieved Novemeber 2018, from https://www.epa.gov/sites/.../files/.../fracturegrowthinlayeredanddiscontinuousmedia.pdf

Warpinski, N. R., Abou-Sayed, I., Moschovidis, Z., & Parker, C. (1993). *Hydraulic Fracture Model Comparison Study_Complete Resuts.* Gas Reaseach Institute, Tight Sands and Gas Processing Research Department. Gas Research Institute.

Weijers, L., De Pater, C. J., Owens, K. A., & Kogsboil, H. H. (1994, May). Geometry of Hydraulic Fractures Induced From Horizontal Wellbores. *One Petro, 9*(02), 87-92. doi:https://doi.org/10.2118/25049-PA

Xiang, J. (2011). *A PKN hydraulic fracture study and formation permeability determination.* MSc Thesis, Texas A&M University. Retrieved July 2017, from http://oaktrust.library.tamu.edu/bitstream/handle/1969.1/ETD-TAMU-2011-12-10212/XIANG-THESIS.pdf?sequence=2

Xiphu, M. R., Mills, S. R., Chevallier, L., Marot, J., Mkhize, M., Motloung, T., . . . van Wyk, E. (2012). *Report on the investigation of hydraulic fracturing in the Karoo Basin of South Africa.* Department of Mineral Resources. Retrieved April 11, 2017, from http://www.dmr.gov.za/publications/viewcategory/182-report-on-hydraulic-fracturing.html

Yew, C. H., & Weng, X. (2015). *Mechanics of Hydraulic Fracturing* (2nd ed.). Oxford: Elsevier.

Yildrium, L. (2014). *Evaluation of petrophysical proerties of gas shale and their change due to interaction with water.* MSc Thesis, The Pennslyvania State University, College of Energy and Mineral Engineering. Retrieved January 2018, from https://etda.libraries.psu.edu/files/final_submissions/10190

Zhao, H., Li, Z., Zhu, C., & Ru, Z. (2018). Reliability analysis models for hydraulic fracturing. *Journal of Petroleum Science and Engineering, 162*, 150-157. Retrieved 11 24, 2018, from https://sciencedirect.com/science/article/pii/s0920410517310057

Appendices

A. General pressure profile for Hydraulic Fracturing

Hydraulically induced fractures propagate from the wellbore into reservoir as pumping continues. Figure A1 shows a typical downhole pressure record (i.e., the pressure measured inside the hole near the opening of hydraulic fracture). As the fracture propagates into the reservoir, the frac-fluid leaks off from the fracture surface into the surrounding rock medium at the same time. The opening of the fracture is maintained by the net pressure (fluid pressure minus the minimum in situ stress), while the fluid leak-off rate from the fracture surface is caused by the differential between fluid pressure and reservoir pressure.

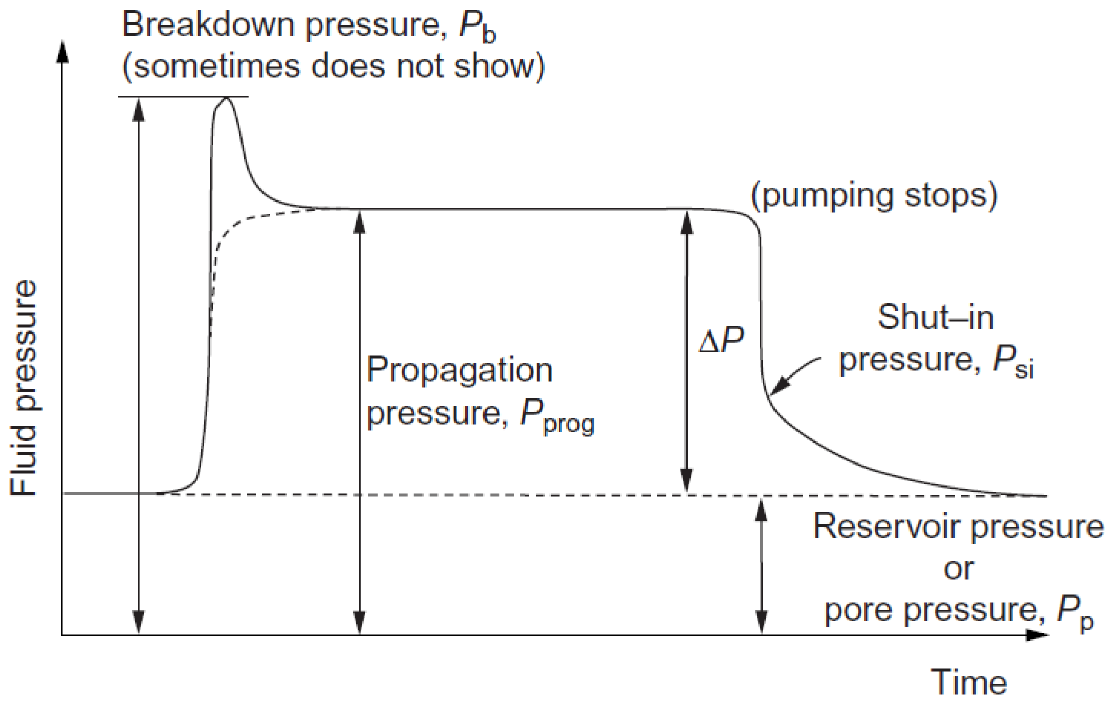

Figure A. 1: A typical downhole pressure record (Hattori, Trevelyan, Augarde, Coombs, & Aplin, 2017)

Referring to Figure A1, the maximum pressure is the initial breakdown pressure P_b. The pressure drops, but not always in the field, when a fracture is initiated at the borehole surface. The near constant portion of the pressure curve is the propagation pressure P_{prog}. This is the pressure that causes the propagation of hydraulic fracture into the reservoir. When pumping stops, the pressure drops instantly to a lower value, due to the vanishing frictional pressure loss in the pipe, perforation entrance and near-borehole area, and then continues to decrease slowly to the reservoir pressure due to fluid leaking off from the fracture and borehole as shown in the Figure. The transition point is called the shut-in pressure psi (or the instantaneous shut-in pressure, ISIP). However, fluid continues to leak off from fracture surface and the fracture opening width continues to decrease. The fluid pressure inside the fracture eventually reaches equilibrium with the minimum in situ stress and at this point the hydraulic fracture closes. The fracture closure pressure, which can be determined from the pressure decline analysis, is taken as a measure of the minimum in situ stress.

B. Matlab code used to obtain fracture growth, 3D prediction and pressure behaviour.

B1. Pressure behaviour with time

```
function fracture2DP3D
%-----------------------------------------------------------------------
G=1.466*1e6;        % Shear modulus        [psi]
v=.2;               % Drained Poisson's ratio
mu=1;               % Fluid viscosity      [cp]
Zi=3200;            % In-situ stress       [psi]
Q=62.5;               % Pumping rate          [bbl/min]
h=2.5;                % Fracture height       [ft]
rw=.2;              % Wellbore radius      [ft]
tf=input('How much time is passed?);
tic;
%************************************************************************
[Tkgd,pkgd]=KGD(tf,G,Q,v,mu,Zi);%           KGD
%************************************************************************
[Tpkn,ppkn]=PKN(tf,G,Q,v,mu,h);%            PKN
%************************************************************************
[T3,p3]=TD(tf,G,Q,mu,Zi,rw,h);%             P3D
%************************************************************************
figure(1)
set(1,'name','WELLBORE PRESSURE vs TIME in 2D and P3D
MODELS','numbertitle','off')
    subplot(311)
       plot(pkgd,Tkgd,'r');
       ylabel('Pressure (psi), KGD Model');
       xlabel('Time (min)');
    subplot(312)
       plot(ppkn,Tpkn,'b')
       ylabel('Net Pressure (psi), PKN Model');
       xlabel('Time (min)');
    subplot(313)
       plot(p3,T3,'m')
       ylabel('Wellbore Pressure (psi), P3D')
       xlabel('Time (min)')
toc
end
```

B2. Fracture growth and 3D prediction for KGD model

```
function [P,T]= KGD(tf,G,Q,v,mu,Zi)
%************************************************************************
%-------------                   KGD                        -------------
%************************************************************************
for t0=tf/50:tf/50:tf       %time step for visualization
i=1;
for t=0:.0001:t0
    ngr(i)=0;
    L(i)=.48*(8*G*Q^3/((1-v)*mu))^(1/6)*t^(2/3);    %Fracture Length
    W0(i)=1.32*(8*(1-v)*mu*Q^3/G)^(1/6)*t^(1/3);    %maximum fracture
opening width
    Pw=Zi+0.96*(2*Q*mu*G^3/((1-v)^3*L(i)^2))^(1/4); %wellbore pressure
    Pwi(i)=Pw;
    time(i)=t;
    i=i+1;
```

```
end
figure(10);
set(10,'name','KGD fracture growth and final shape','numbertitle','off');
drawnow;
limitL=.48*(8*G*Q^3/((1-v)*mu))^(1/6)*tf^(2/3);     %used for axis limits
limitW0=1.32*(8*(1-v)*mu*Q^3/G)^(1/6)*tf^(1/3);
h=1.1*limitL;
     subplot(221);
       plot(time,L,'r');
       ylabel('Length (ft)');
       xlabel('Time (min)');
       axis([0 tf 0 limitL]);
       grid on;
    subplot(222);
        plot(time,W0,'r');
        ylabel('Max Width (in)');
        xlabel('Time (min)');
        axis([0 tf 0 limitW0]);
        grid on;
    subplot(224);
    fL=fliplr(L);
       plot3(fL,W0,ngr,'r');
       hold;
       plot3(fL,-W0,ngr,'r');
       hold;
       axis([0 limitL -2*limitW0 2*limitW0 -1 1]);
       grid on;
      ylabel('Max Width (in)')
      xlabel('Length (ft)')
      set(gca,'ztick',[]);
      daspect([1,1/2,1]);
     view(-62,26);
     grid on;
     hold off;
end
     subplot(223);
     hold;
for I=0:h/100:h
       plot3(fL,W0,ngr+I);
       plot3(fL,-W0,ngr+I);
end
      daspect([1,1/6,1]);
      view(-56,28);
       ylabel('Width (in)')
       zlabel('Height (ft)')
       xlabel('Depth (ft)')
      grid on;
T=time;P=Pwi;
end
```

B3. Fracture growth and 3D prediction for PKN model

```
function [P,T]= PKN(tf,G,Q,v,mu,h)
%*********************************************************************
%-------------            PKN    (Assuming no leak off)          -------
%*********************************************************************
for t0=tf/50:tf/50:tf        %time step for visualization
i=1;
for t=0:.001:t0
    ngr(i)=0;
```

```
    L(i)=.68*(G*Q^3/((1-v)*mu*h^4))^(1/5)*t^(4/5);   %Fracture Length
    W0(i)=2.5*((1-v)*mu*Q^2/(G*h))^(1/5)*t^(1/5);      %Fracture opening
width
    Pw=2.5*(Q^2*mu*G^4/((1-v)^4*h^6))^(1/5)*t^(1/5);   %wellbore net
pressure
    Pwi(i)=Pw;
    time(i)=t;
    i=i+1;
end
timer=fliplr(time);
limitL=.68*(G*Q^3/((1-v)*mu*h^4))^(1/5)*tf^(4/5);    %used for axis limits
limitW0=2.5*((1-v)*mu*Q^2/(G*h))^(1/5)*tf^(1/5);
h2=0.2*limitL;
z=h2/time(end).*time+h2/2;
A=G*Q^3/((1-v)*mu*h2^4);a=.68^(5/4)*A;
B=((1-v)*mu*Q^2)/(G*h2);b=2.5^5*B;
c=h2/time(end);Z=z-h2/2-t0*c;
figure(20)
set(20,'name','PKN frac growth and entrance','numbertitle','off')
drawnow;
     subplot(221)
       plot(time,L)
       ylabel('Length (ft)')
       xlabel('Time (min)')
       axis([0 tf 0 limitL])
       grid on;
    subplot(222)
        plot(time,W0)
        ylabel('Max Width (in)')
        xlabel('Time (min)')
        axis([0 tf 0 limitW0])
        grid on;
    subplot(224)
       fL=fliplr(L);
       plot3(fL,W0,ngr,'b');
       hold;
       plot3(fL,-W0,ngr,'b');
       hold;
       axis([0 limitL -2*limitW0 2*limitW0 -1 1]);
       grid on;
       ylabel('Width (in)')
       xlabel('Length (ft)')
       set(gca,'ztick',[]);
       daspect([1,1/2,1]);
     view(-53,56)
     hold off;
end
figure(20)
    subplot(223)
       plot3(ngr,W0,-z+1.5*h2,'b');
       hold;
       plot3(ngr,-W0,-z+1.5*h2,'b');
       plot3(ngr,W0,z-1.5*h2,'b');
       plot3(ngr,-W0,z-1.5*h2,'b');
       axis([-1 1 -2*limitW0 2*limitW0 -2*h2 2*h2]);
       grid on;
       ylabel('Width (in)')
       zlabel('Height (ft)')
       set(gca,'xtick',[]);
       daspect([1,1,1]);
     view(-60,20)
```

```
     hold off;
figure(21)
set(21,'name','PKN final shape','numbertitle','off')
hold;

for I=0:h2/100:h2
       plot3(fL,W0,ngr+I,'g');
       plot3(fL,-W0,ngr+I,'b');
       plot3(fL,W0,-ngr-I,'g');
       plot3(fL,-W0,-ngr-I,'b');
       grid on;
       ylabel('Width (in)')
       zlabel('Height (ft)')
       xlabel('Depth (ft)')
       set(gca,'ytick',[]);
       daspect([1,5.5,1]);
     view(-77,4)
end
       plot3(ngr,W0,-z+1.5*h2,'r*');
       plot3(ngr,-W0,-z+1.5*h2,'r*');
       plot3(ngr,W0,z-1.5*h2,'r*');
       plot3(ngr,-W0,z-1.5*h2,'r*');
       grid on;

T=time;P=Pwi;
end
```

B4. Fracture growth for P3D model

```
function [P,T]= TD(tf,G,Q,mu,Zi,rw,h)
%***************************************************************************
%-------------          Geertsma de Klerk    (P3D)                -------
%***************************************************************************
for t0=tf/50:tf/50:tf        %time step for visualization
i=1;
for t=0:.001:t0
    ngr(i)=0;
    R(i)=.548*(G*Q^3/mu)^(1/9)*t^(4/9);            %Fracture radius
    W0(i)=21*(mu^2*Q^3/G^2)^(1/9)*t^(1/9);         %Maximum fracture opening
width
    Pw=Zi-5/(4*pi)*(G*W0(i)/R(i))*log(rw/R(i));    %wellbore net pressure
    Pwi(i)=Pw;
    time(i)=t;
    i=i+1;
end
figure(30)
    set(30,'name','P3D fracure growth-(R vs t)  (W vs
t)','numbertitle','off')
    drawnow;
    limitRi=.548*(G*Q^3/mu)^(1/9)*tf^(4/9);     %used for axis limits
    limitW0=21*(mu^2*Q^3/G^2)^(1/9)*tf^(1/9);
    subplot(221)
       ezplot(sprintf('z.^2/%f +x.^2/%f -1',(h/2)^2,(R(end))^2),[-0 limitRi
-h h]);
       ylabel('Height (ft)')
       xlabel('Depth (ft)')
    subplot(222)
       ezplot(sprintf('z.^2/%f +y.^2/%f -1',(h/2)^2,(W0(end)/2)^2),[-
limitW0 limitW0 -h h]);
       ylabel('Heigth (ft)')
```

```
        xlabel('Width (in)')
        daspect([12,1,1]);
        set(gca,'xtick',[])
     subplot(224)
        hold;
        A=R(end);B=W0(end)/2;C=h/2;
        tp = linspace(0,2*pi,100);
        pp = linspace(0,pi,100);
        [T,P] = meshgrid(tp,pp);
        x = A*cos(T).*cos(P);
        y = B*cos(T).*sin(P);
        z = C*sin(T);
        surf(x,y,z);
        daspect([1,6,1]);
        view(-51,22)
        xlabel('Depth (ft)');
        ylabel('Width (in)');
        zlabel('Height (ft])');
        axis([0,limitRi,-limitW0,limitW0,-h/2,h/2]);
end
        clearvars ngr tp tt T P y z i
        tp = linspace(0,2*pi,1000);
        pp = linspace(0,pi,1000);
        [T,P] = meshgrid(tp,pp);
        y = B*cos(T).*sin(P);
        z= C*sin(T);
        for i=1:length(y)
            ngr(i)=0;
        end
        hold;
        plot3(ngr,y,z,'m')
        daspect([1,6,1]);
        view(-51,22)
        grid on;
T=time;P=Pwi;
end
```

C. Constant Height Models:

There are two basic constant height models: the Khristianovic-Geertsma-de Klerk (KGD) model, and the Perkins-Kern-Nordgren (PKN) model. Most of the early hydraulic fractures were designed by applying one of these models. The underlying mechanics in these two models, however, differs significantly (Yew & Weng, 2015).

C1. The KGD model

One wing of the KGD fracture is shown in Figure C! . In addition to the constant height assumption, two other assumptions are (1) the fracture is at a plane strain condition in the horizontal plane; and (2) the fracture tip is a cusp-shaped tip as proposed by Barenblatt [12]. This assumption of a cusp-shaped tip removes the stress singularity at the fracture tip that would otherwise be predicted by the elasticity analysis. Following Geertsma-de Klerk, the fracture is approximated as a channel of opening width w. The pressure distribution for the flow of a viscous fluid (Newtonian fluid) inside the fracture can be written as

$$p_w - p = \frac{12\mu QL}{h}\int_{f_{LW}}^{f_L}\frac{df_L}{w^3} \quad \text{[Equation C1]}$$

Where:

- $f_L = x/L$
- $f_{LW} = r_W/L$
- h = fracture height
- L = total length of the fracture
- p = local fluid pressure
- p_W = fluid pressure at wellbore
- Q = fluid injection rate into one wing of the fracture
- r_W = wellbore radius
- w = local fracture width
- μ = frac fluid viscosity

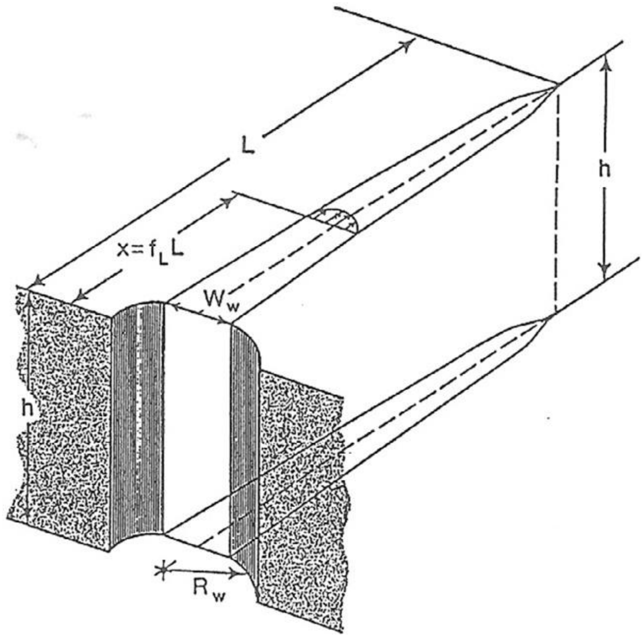

Figure C. 1: Sketch of the KGD constant height model (Yew & Weng, 2015).

Equation C1 has two unknowns, p and w. England and Green's solution (1963) for a plane fracture in an infinite elastic medium provides another relationship between p and w as:

$$w = \frac{4(1-v)L}{\pi G}\left[\int_{f_L}^{1} \frac{f_2 df_2}{\sqrt{f_2^2 - f_L^2}} \int_0^{f_2} \frac{p(f_1)df_1}{\sqrt{f_2^2 - f_1^2}} - \frac{\pi}{2}\sigma_{min}\sqrt{1-f_L^2}\right] \qquad \text{[Equation C2]}$$

Where:

- G = shear modulus of the rock
- v = Poisson's ratio or the rock
- f_1 and f_2 = the fraction of the fraction extent ($=x/L$)
- σ_{min} = minimum in-situ stress

Equation C2 is derived using the elasticity theory.

The time history of fracture width w(t) and fluid pressure p(t) can be obtained by solving Equations C1 and C2 with proper boundary conditions. The following smooth fracture tip condition proposed by Barenblatt (1962) is used by Geertsma and de Klerk:

$$\left(\frac{dw}{df_L}\right)_{f_L=1} = 0 \qquad \text{[Equation C3]}$$

The same condition is also used by Khristianovic and Zheltov (1955) in their study of hydraulic fracturing. The proper boundary condition at the fracture tip should be f_L = 1 , w = 0, not as in Equation C3. Therefore, there is a mathematical inconsistency at the fracture tip.

By assuming that the dry zone in front of fracture tip is small and that the shape of wet portion in the fracture can be approximated by an ellipse, the following approximate solutions (no fluid leak off) are obtained by Geertsma and de Klerk:

Fracture length

$$L = 0.48\left[\frac{8GQ^3}{(1-v)\mu}\right]^{1/6} t^{2/3} \qquad \text{[Equation C4]}$$

Maximum fracture opening width

$$w_o = 1.32\left[\frac{8(1-v)Q^3\mu}{G}\right]^{1/6} t^{1/3} \qquad \text{[Equation C5]}$$

Wellbore pressure

$$p_w = \sigma_{min} + 0.96\left[\frac{2G^3Q\mu}{(1-v)^3L^2}\right]^{1/4} \qquad \text{[Equation C6]}$$

C2. The PKN model

Figure C1 is a sketch of a PKN fracture. In addition to assuming a constant fracture height, the other two assumptions are:

(1) the fracture is at a state of plane strain in the vertical plane and the vertical fracture cross-section is elliptical and

(2) the fracture toughness has no effect on the fracture geometry, that is, the KIC of the rock medium is assumed to be zero.

The continuity equation for flow of an incompressible fluid inside the fracture, following Nordgren (1972), can be written as:

$$\frac{\partial q}{\partial x} + q_l + \frac{\partial A}{\partial t} = 0 \qquad \text{[Equation C7]}$$

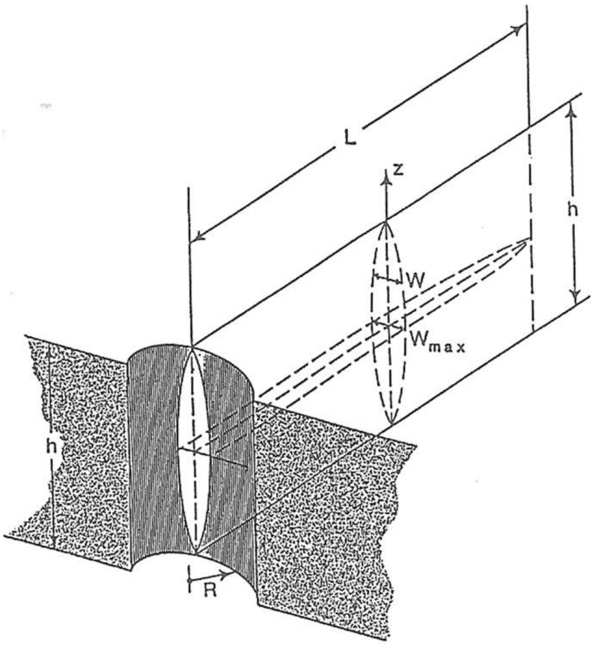

Figure C. 2: Sketch of the PKN constant height model (Yew & Weng, 2015).

Where:

- $q(x,t)$ = volume rate of flow through a cross-section of the fracture.
- $q_l(x,t)$ = volume rate of fluid leak-off per unit of fracture length
- $A(x,t)$ = cross-sectional area of the fracture

The elliptical fracture opening width w is directly related to the net pressure p by Equation C8 :

$$w = \frac{(1-v)}{G}\sqrt{h^2 - 4z^2}\, p \quad \text{[Equation C8]}$$

Knowing the fracture geometry, the fracture cross-sectional area can be written as:

$$A = \int_{-h/2}^{h/2} w dz = \frac{\pi}{4} Wh \quad \text{[Equation C9]}$$

Where:

- $W = w_{max}$ is the maximum fracture opening width.

The volume rate of fluid flow q is related to the pressure gradient by the solution for laminar flow of Newtonian fluid in an elliptical tube, that is,

$$q = -\frac{\pi W^3 h}{64\mu}\frac{\partial p}{\partial x} \quad \text{[Equation C10]}$$

The fluid leak-off rate, q_l, is expressed as:

$q_l = \frac{2c_l h}{\sqrt{t-\tau(x)}}$ [Equation C11]

Where:

- c_l = the fluid loss coefficient
- $\tau(x)$ = time at which fluid leak-off begins at position x

Substituting of equations C9-C11 into Equation C7 gives the governing equation for the propagation of a hydraulically induced fracture, Equation C12 :

$\frac{G}{64(1-v)\mu h}\frac{\partial^2 W^4}{\partial x^2} = \frac{8c_l}{\pi\sqrt{t-\tau(x)}} + \frac{\partial W}{\partial t}$ [Equation C12]

The initial condition for Equation C12 is:

$$W(x,0) = 0$$

and the boundary conditions are:

$$W(x,t) = 0 \; at \; x \geq L(t)$$

$$\left[\frac{\partial W^4}{\partial t}\right]_{x=0} = -\frac{256(1-v)\mu}{\pi G}Q$$

The above equations are then solved numerically for specific conditions.

D. Additional Information

Table D. 1: Top 10 countries with technically recoverable shale gas resources (Nguyen, 2016).

Country	Shale gas resource (trillion cubic feet (Tcf))
China	1275
USA	862
Argentina	774
Mexico	681
South Africa	785
Australia	396
Canada	388
Libya	290
Algeria	231
Brazil	226

Table D. 2: Fracturing fluids and conditions for their use (Frink, 2013)

Base Fluid	**Fluid Type**	**Main Composition**	**Usages**
Water			
	Linear	Guar, HPG, HEC, CMHPG	Short fractures, low temperature
	Crosslinked	Crosslinker + Guar, HPG, CMHPG or CMHEC	Long fractures, high temperature
	Micellar	Electrolyte + Surfactant	Moderate length fractures, moderate temperature
Foam			
	Water based	Foamer + N_2 or CO_2	Low-pressure formations
	Acid based	Foamer + N_2	Low-pressure, carbonate formations
	Alcohol based	Methanol + Foamer + N_2	Low-pressure, water-sensitive formations
Oil			
	Linear	Gelling agent	Short fractures, water-sensitive formations

	Crosslinked	Gelling agent + Crosslinker	Long fractures, water-sensitive formations
	Water emulsion	Water + Oil + Emulsifier	Moderate length fractures, good fluid loss control
Acid			
	Linear	Guar or HPG	Short fractures, carbonate formations
	Crosslinked	Crosslinker + Guar or HPG	Longer, wider fractures, carbonate formations
	Oil emulsion	Acid + Oil + Emulsifier	Moderate length fractures, carbonate formations

Table D. 3: Equations and outline of the 2D and 3D models (Perkins & Kern, 1961, Zhao, Li, Zhu, & Ru, 2018)

Model:KGD/2D Equations: $L=0.48\left(\frac{8GQ^3}{(1-\nu)\mu}\right)^{(1/6)}.t^{(2/3)}$ $W_o=1.32\left(\frac{8(1-\nu)Q^3\mu}{G}\right)^{(1/6)}.t^{(1/3)}$ $Pw=\sigma_{min}+0.96\left(\frac{2G^3Q\mu}{(1-\nu)^3L^2}\right)^{(1/4)}$	*The model is best suited for fractures whose length/height ratio is near unity or less.* Hence: Height=1.1*final length **Assumptions** -Constant height assumption -The fracture is at a plane strain condition in the horizontal plane -The fracture tip is a cusp-shaped tip -Hydraulic fracture fluid is viscous and Newtonian -Elasticity theory applied -No leak off	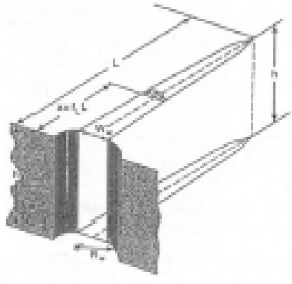 The KGD constant height fracture model.
Model:PKN/2D Equations: $L=\left(\frac{Q}{\pi c_l h}\right)t^{(1/2)}$ $W_o=4\left(\frac{2(1-\nu)Q^2\mu}{\pi^3 G c_l h}\right)^{(1/4)}.t^{(1/8)}$ $Pw=2.5\left(\frac{G^4Q^2\mu}{(1-\nu)^4h^6}\right)^{(1/5)}.t^{(1/5)}$	*The model is generally regarded to be best suited for fractures whose length/height ratio is large.* Hence: Height=0.2*final length **Assumptions:** -The fracture is at a state of plane strain in the vertical plane and the vertical fracture cross-section is elliptical -The fracture toughness has no effect on the fracture geometry -No leak off	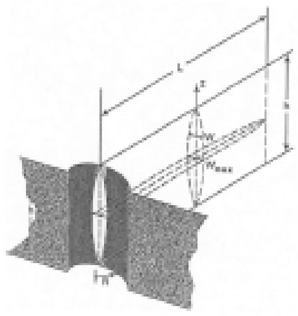 The PKN constant height fracture model.
Model:Modified P3D Equations: $Peneterationdepth(R)=0.548\left(\frac{GQ^3}{\mu}\right)^{(1/9)}.t^{(1/9)}$ $W_o=1.32\left(\frac{8(1-\nu)Q^3\mu}{G}\right)^{(1/6)}.t^{(1/3)}$ $Pw=\sigma_{min}-\frac{5}{4\pi}\frac{Gw_o}{R}\ln\frac{(r_w)}{R}$	Constant Height=3 ft. **Assumptions:** -Vertical distribution of the minimum in-situ stress is uniform. -Fracture growth follows elliptical shape. -No leak off	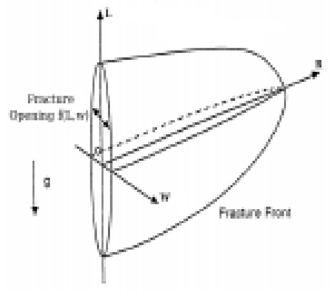 The predicted 3D shape of the fracture